From DARPins to LoopDARPins: Novel LoopDARPin Design Allows the Selection of Low Picomolar Binders in a Single Round of Ribosome Display

Johannes Schilling, Jendrik Schöppe and Andreas Plückthun

Biochemisches Institut, *Universität Zürich, Winterthurerstrasse 190, CH-8057 Zürich, Switzerland*

Correspondence to Andreas Plückthun: *plueckthun@bioc.uzh.ch*
http://dx.doi.org/10.1016/j.jmb.2013.10.026
Edited by S. Koide

Abstract

Antibodies are the most versatile binding proteins in nature with six loops creating a flexible continuous interaction surface. However, in some molecular formats, antibodies are aggregation prone. Designed ankyrin repeat proteins (DARPins) were successfully created as alternative design solutions. Nevertheless, their concave shape, rigidity and incompletely randomized binding surface may limit the epitopes that can be targeted by this extremely stable scaffold. Combining conformational diversity and a continuous convex paratope found in many antibodies with the beneficial biophysical properties of DARPins, we created LoopDARPins, a next generation of DARPins with extended epitope binding properties. We employed X-ray structure determination of a LoopDARPin for design validation. Biophysical characterizations show that the introduction of an elongated loop through consensus design does not decrease the stability of the scaffold, consistent with molecular dynamics simulations. Ribosome-display selections against extracellular signal-regulated kinase 2 (ERK2) and four members of the BCL-2 family (BCL-2, BCL-XL, BCL-W and MCL-1) of anti-apoptotic regulators yielded LoopDARPins with affinities in the mid-picomolar to low nanomolar range against all targets. The BCL-2 family binders block the interaction with their natural interaction partner and will be valuable reagents to test the apoptotic response in functional assays. With the LoopDARPin scaffold, binders for BCL-2 with an affinity of 30 pM were isolated with only a single round of ribosome display, an enrichment that has not been described for any scaffold. Identical stringent one-round selections with conventional DARPins without loop yielded no binders. The LoopDARPin scaffold may become a highly valuable tool for biotechnological high-throughput applications.

Introduction

The fast generation of high-affinity protein-based binders used as components of future therapeutics, diagnostic reagents or in research as inhibitors, probes or co-crystallization agents has become more and more important in the recent past. For many targets, however, no specific reagents exist.

The *in vitro* selection of binding proteins is generally faster than the *in vivo* generation of antibodies by the immunization of animals. However, selection is still often the limiting step in the creation of binders. Improvements that accelerate the selection process are thus of greatest importance, especially with respect to high-throughput applications, and the quality of the library from which the selection takes place may be the single most important parameter. We therefore aimed to develop a scaffold with which rapid binder generation is possible without compromising on affinity or specificity.

A variety of technologies developed for recombinant antibody libraries [1–3] allow us to specifically select binders. However, the application of antibody fragments can be limited, since they often lack sufficient conformational stability under harsh conditions, as their domain architecture, a β-sandwich, can be aggregation prone in the context of some molecular formats. Moreover, stabilizing intra-domain disulfide bonds in their framework in general interfere with their functional expression in the reducing intracellular environment in cellular assays ("intrabodies") [4]. New protein scaffolds for molecular recognition

have been developed to overcome these limitations [4–6]. One of these promising new scaffolds are designed ankyrin repeat proteins (DARPins), which were derived from natural ankyrin repeat (AR) proteins by consensus design [7]. AR proteins are involved in important protein–protein interactions in practically all species [8,9], and their modular nature allows high-affinity interactions to binding partners [4,5,10,11].

The original DARPin scaffold was created through a consensus design approach, utilizing the great abundance of natural AR proteins. Conserved intra- and inter-repeat interactions characteristic for the AR domain fold were determined, and conserved framework residues were fixed and potential target interaction residues were randomized in the resulting 33-amino-acid consensus AR. The elongation of a single module by stacking of self-compatible repeats finally yielded a rod-shaped repeat protein, which was sealed at both ends by capping repeats, being hydrophilic on the outside and hydrophobic toward the internal repeats. Well-expressed and extremely stable [4,6,7,12] DARPins have been selected against many targets in the past [7,13–22].

Nonetheless, the most versatile binding proteins in nature are antibodies. Their antigen-binding sites consist of six loops, connecting the strands of β-sheets in the variable domains of the light and heavy chain [23]. Five of the six loops adopt a discrete repertoire of main-chain conformations [24–32]. The loop of the third hypervariable region of the heavy chain (CDR-H3 loop), however, shows much greater variability in length, sequence and conformation than the other five antigen-binding loops and is therefore an important source of antibody diversity [33,34]. Nonetheless, structural analysis of different CDR-H3 loops identified common structural patterns within the basis of the loop, although the tip of the loop differed considerably [23,35]. Interestingly, the CDR-H3 loop plays a crucial role in antigen recognition [36,37], sometimes by changing its conformation upon binding [38–40].

The success of the original DARPin design in routinely generating highly specific binders against a multitude of targets with very different properties has been demonstrated in numerous studies [4–6]. Thus, we decided to use DARPins as the starting point for our new design. Target binding by DARPins is governed by rigid-body interactions, and conformational changes of the DARPin backbone do not occur on binding [13]. Although this mode of binding is entropically favored, we hypothesized that some epitopes on target proteins might be accommodated more easily through a higher degree of flexibility and a larger interaction surface and that, together with a distinctly different surface shape, the number of accessible epitopes might be greatly increased, allowing high-affinity binding in many cases.

Inspired by the antibody CDR-H3 loop region [33,34], we combined the design feature of conformational diversity found in antibodies with the beneficial biophysical properties of the successful DARPin scaffold and engineered a 19-amino-acid loop consensus sequence into the existing DARPin scaffold at the original β-turn position to yield LoopDARPins (Fig. 1). The design challenge was to avoid that a large random loop would destabilize the otherwise extremely favorable biophysical properties of the scaffold. To further extend the interaction surface and to make it continuous, we also randomized the previously unrandomized N- and C-capping repeats and combined them with our LoopDARPin library (Fig. 1).

Here we describe the design, construction, analysis and experimental structure verification of these new LoopDARPin libraries. We show that our design was successful and demonstrate that, with LoopDARPins, we have generated a scaffold, which possesses the conformational flexibility and biophysical properties that we aimed at creating. We also investigated the ability of the LoopDARPin scaffold to rapidly yield binders under extremely stringent selection conditions (Fig. 2). We show that we were able to select a variety of well-behaved, specific, high-affinity LoopDARPins with K_D values in the picomolar range, using a minimal number of highly stringent ribosome-display [41,42] selection rounds against five globular eukaryotic proteins at unparalleled speed, emphasizing the great potential of the LoopDARPin scaffold.

Results

Identification of a loop consensus sequence through sequence databases

As a first step in the LoopDARPin design, a loop of 10–20 amino acids in length that maintained the integrity of the framework had to be devised. Inspired by nature, we aimed at creating a loop with a stabilizing defined stem as in the antibody CDR-H3 loop and in natural ankyrin repeat proteins that possess loop insertions [23,31,32,35,43–46]. Since sequence and structure conservation among ARs is high, we employed a consensus design strategy to identify a loop consensus sequence composed of fixed stabilizing framework positions and randomized potential interaction positions.

Structural considerations of the DARPin fold led us to the conclusion that the most promising position for the insertion of a longer loop into the existing DARPin scaffold was the protruding β-turns (Fig. 1). It is at these positions that a protruding loop would have a high probability to contact the target.

We summarize here the results of the design, and a detailed description of the applied loop consensus design can be found in Supplementary Results. To accumulate enough sequence and structural information for our loop consensus design, we identified lead structures for further sequence analyses using

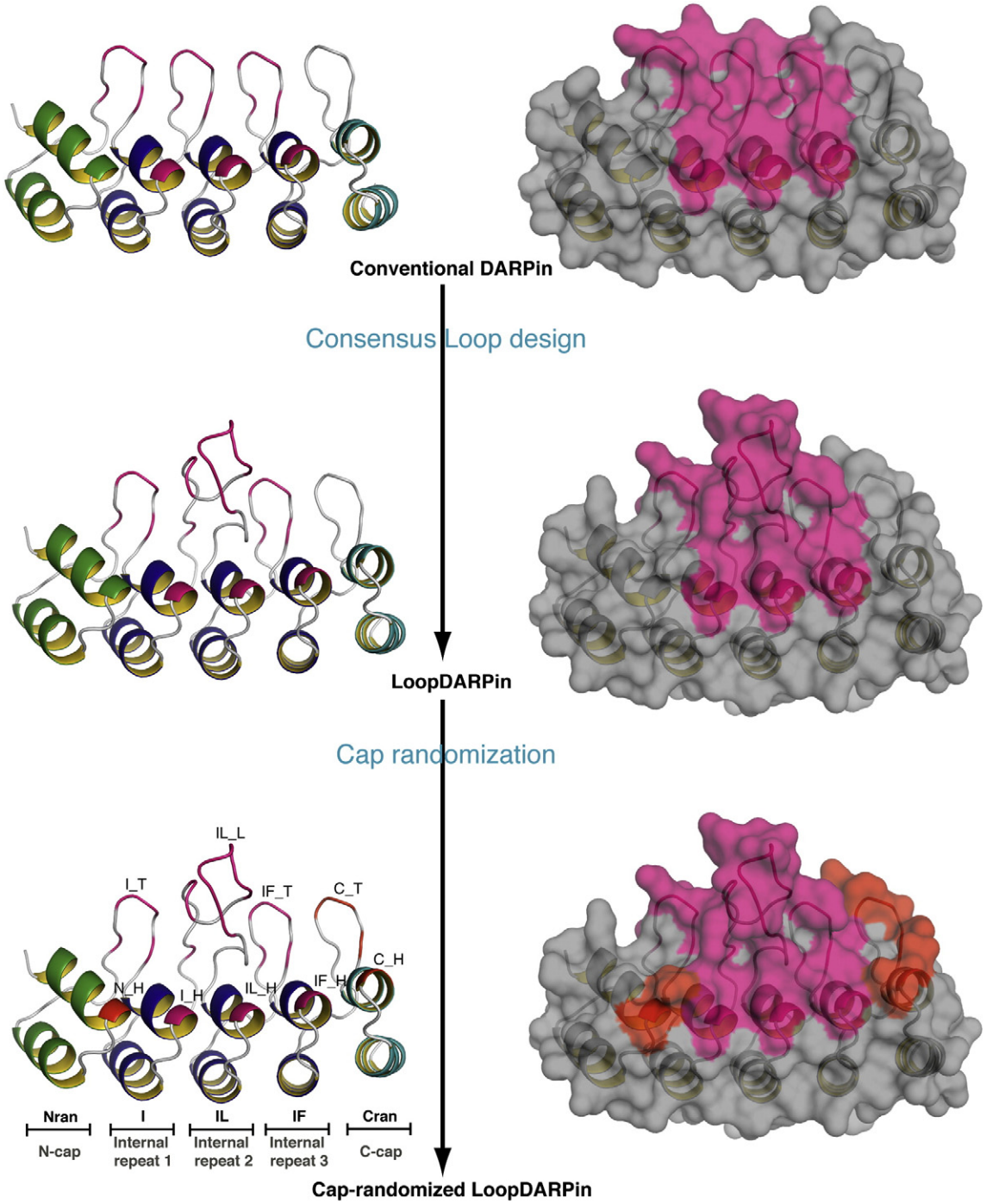

Fig. 1. Overview of the applied strategy to engineer conventional DARPins into LoopDARPins and further into cap-randomized LoopDARPins. The structures of a conventional DARPin (PDB ID: 2XEE) (top) and a modeled energy-minimized structure of a LoopDARPin with three internal consensus repeats harboring an elongated loop in the second internal module (middle and bottom) are shown in ribbon and surface representation. Helices of the N-terminal capping repeat, the internal repeat modules and the C-terminal capping repeat are colored green, blue and cyan, respectively. The complete designations of the individual repeat modules are given below the lower modeled structure, and abbreviations are shown in the structure. Randomized positions of the N-terminal capping repeat (N-cap, denoted N_{ran}) and the C-terminal capping repeat (C-cap, denoted C_{ran}) are colored red. Randomized positions of the three internal repeat modules (I, internal repeat; IL, loop-containing internal repeat; IF, loop-following internal repeat) are colored pink. Uniformly used abbreviations are given next to the colored patches, with the ending *_H* for randomized positions in helical parts and *_T* for the β-turns, to facilitate denoting the structural position of the randomized positions in the amino acid sequence alignments (Fig. S3). Randomized positions of the loop are marked with *IL_L*. This figure was created with the help of PyMOL[¶].

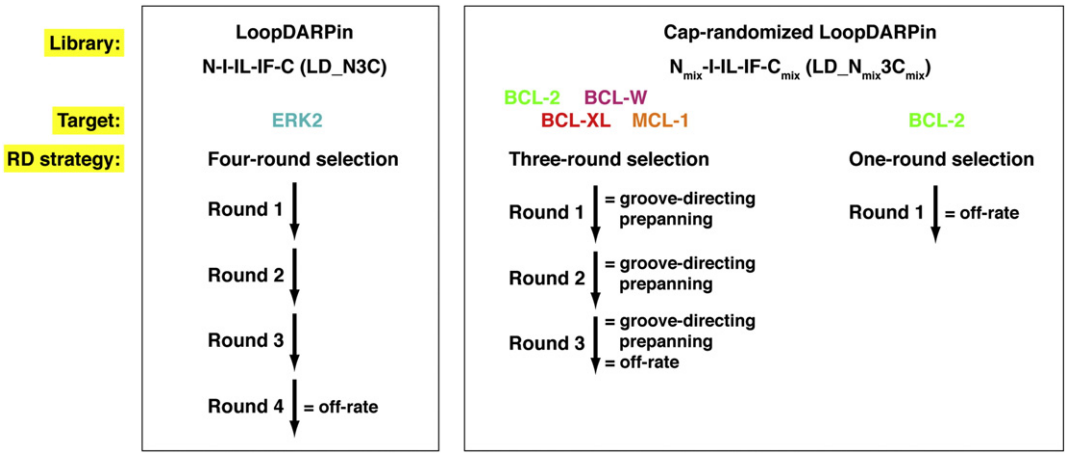

Fig. 2. Overview of the strategy used to test the performance of our newly created LoopDARPin libraries in rapidly selecting high-affinity binders against multiple target proteins.

the three-dimensional structure of DARPin 2XEE [47] in a BLAST search against the PDB. Seven natural AR lead structures with an insertion of varying length at one or more β-turns were found. Structural investigations of all lead structures revealed that each of them could in principle serve as a separate starting point for a consensus loop design. Therefore, the sequence of each of the obtained hit structures was subsequently used in a separate BLAST search against GenBank to retrieve individual sequence data sets for a consensus sequence analysis step and to delineate the natural variety of the particular ankyrin protein.

To focus the BLAST search on the β-turn region but, at the same time, to include a proper amount of natural AR repeat sequence in our search, for each lead sequence, we used a minimal search sequence including the helix1-helix2-turn-helix1-helix2 motive (Fig. 3b).

Most structural and sequence data were obtained for the 2F37 lead structure. The 86 BLAST hits obtained for this lead were then manually aligned and analyzed, yielding loop consensus A (Fig. 3a).

Refinement of loop consensus A using structural data

Positions in the loop consensus A crucial for the structural integrity of the loop and positions suitable for randomization needed to be identified. We therefore extended our sequence database analysis and included structural data in our final refinement, leading to loop consensus B (Fig. 3a and b).

The 2F37 lead structure is that of a natural AR, which is part of the conserved N-terminal intracellular domain of all transient receptor potential (TRP) channels of the vanilloid receptor subfamily (TRPV). Structures have been solved for TRPV1 (2PNN) [43], rat TRPV2 (structures from two crystal forms: 2ETB and 2ETC) [44], human TRPV2 (2F37) [45] and TRPV6 (2RFA) [46] (Fig. 3b). Since sequences of all of these structures were included in the 86 BLAST hits, yielding loop consensus A, and since they all possess insertions of similar length at equal positions of the β-turn, structural information from all of these structures was used in our design refinement.

All five structures were structurally aligned with the original DARPin 2XEE. It became immediately apparent that the aligned hit structures all share a structurally conserved stem (blue) and a structurally diverse tip of the loop (pink) (Fig. 3b). The conserved hydrophobic stem of the loop consists of positions 1–3, which engage positions 6, 7 and 16–19 through a network of H-bonds and hydrophobic interactions. Positions 6 and 7 maintain positions 4 and 5 in a rather conserved conformation, although positions 4 and 5 are not involved in stabilizing contacts and instead point toward the solvent. Together with positions 8–15, they are potential target interaction residues, since they appear to be either conformationally flexible or point away from the DARPin body (Fig. 3b). In an extensive structural analysis, described in Supplementary Results in detail, fixed framework positions necessary for structural integrity and positions capable of interacting with a potential target were identified and included in the definition of loop consensus B (Fig. 3a and b).

Reduction of clashes to neighboring repeats

Due to the large dimensions of our loop, we decided to only insert one of these loops into the existing DARPin scaffold. The best position where a β-turn might be exchanged for such a large loop was reasoned to be a central place and, thus, the second internal repeat in a DARPin containing three internal repeats. Thus, the loop would be surrounded by randomized β-turns of neighboring repeats, creating a continuous interaction surface with a protrusion in

the middle, and the stem of our loop could be stabilized by well-placed hydrophobic contacts of the remaining repeat to adjacent repeats (Figs. 1 and 3b).

Modeling of the consensus loop structure into the existing DARPin scaffold identified no clashes between loop and adjacent repeats. However, presuming that a randomized loop might sample a large conformational space, we decided to introduce flexibility into the β-turn of the following repeat (IF-repeat, where I stands for *i*nternal and F stands for loop-*f*ollowing repeat), since we observed the closest distance between loop and adjacent repeats at this position. To accommodate a higher degree of flexibility in the following β-turn, we exchanged Asp1 to an Ala, thereby disrupting the H-bond network (see below). We reasoned that the intrinsic stability of the DARPin would withstand this change, as DARPins were designed to be stable after all.

The final loop consensus B is shown in Fig. 3a. It was designed as a loop that could be inserted into the existing DARPin framework without much reengineering of the DARPin structure. Thus, in this new design, a β-turn of 5 amino acids harboring 3 randomized positions in the original DARPin was replaced by a 19-amino-acid loop with 10 randomized positions, thereby massively increasing the interaction surface of the DARPin (Fig. 3a).

To create a structural model for subsequent analyses and library design, we modeled the final consensus LoopDARPin using InsightII. Coordinates for non-loop positions were taken from the DARPin structure 2XEE. Position 1 in the IF-repeat β-turn was mutated to Ala. For the loop, a sequence rich in Tyr and Ser was used, as these are known to favor protein binding [48–56] (see below). Coordinates for modeling the loop sequence ATG SY FQ YSSSYYVY YFGE were derived from the 2PNN structure. The final consensus LoopDARPin model is shown in Fig. 1.

Randomization of capping repeats

In the original DARPin library, capping repeats were not randomized. Unrandomized caps, however, may disrupt the continuous interaction surface (Fig. 1) and might inhibit target binding for a number of library members. Not surprisingly, the analysis of available DARPin–target complex structures showed that selected DARPins either engage or completely exclude their unrandomized caps from binding the target, emphasizing the great importance of providing a continuous interaction surface. Thus, positions in the N- and C-cap, which correspond to randomized positions in internal repeats, were chosen for randomization. In the N-cap, we randomized positions 11 and 12, located at the end of helix1, to yield the N-cap library N_{ran}. The C-cap library C_{ran} was designed to include randomization of β-turn positions 2, 3 and 5, together with helix1 positions 13 and 14 (Fig. 1 and Fig. S1). Randomizing capping repeats, however, is not without risk, since unfolding of the caps would expose the hydrophobic core of LoopDARPins. It was thus important to validate this design both structurally and by biophysical analyses (see below).

Testing the LoopDARPin design using molecular dynamics simulation

Using molecular dynamics simulations in explicit water, we simulated the consensus LoopDARPin for 50 ns at 300 K using the GROMOS 45A4 force field. The flexibility of the LoopDARPin was examined by analyzing root-mean-square fluctuations (RMSFs) around the average structure. Figure 3c shows that the overall mobility of the consensus LoopDARPin is low. The most flexible regions are located at the termini and at the tip of the loop. Stability at the stem of the loop is retained and permits the tip of the loop to sample a vast conformational space. The given results are consistent with our design goal that our loop consensus should allow the introduction of a conformationally flexible loop into the existing DARPin scaffold without perturbing its structural integrity. The key feature by which this was designed was to keep the stem constant.

Assembly of LoopDARPin DNA libraries

The loop consensus B peptide sequence was back-translated into DNA using optimal *Escherichia coli* expression codons. All codons of the randomized positions were encoded by trinucleotides to ensure maximal library quality with a defined mixture of specific base triplets [57]. The randomization strategy for the previously described designed AR module [7] guarantees a well-balanced ratio between hydrophilic and hydrophobic residues by offering sufficient hydrophobic DARPin–target interactions while simultaneously maintaining solubility. Therefore, this randomization strategy was used for all non-loop positions. At these non-loop positions, we thus allowed A, D, E, H, K, N, Q, R, S and T with 7% probability each and F, I, L, M, V, W and Y with 4.3% probability each.

With our loop randomization strategy, we aimed at reducing non-functional loop structures but, at the same time, making high-affinity binding and conformational flexibility possible. Given the ability of Tyr to participate in H-bonds and in hydrophobic interactions, combining Tyr with Ser and Gly (to allow Tyr flexibility and for making additional interactions) in minimalistic loop libraries has proven successful in the past [48–56]. Tyrosine is also highly overrepresented in antibody-binding sites [58–62]. To achieve sufficient shape diversity and chemical diversity within the limited sequence space of the loop, we therefore biased randomized loop positions toward Tyr (25%), Ser (25%) and Gly (10%). However, all

remaining amino acids except Cys were still allowed with a probability of 2.5% each.

Additional novel design features introduced in our LoopDARPin library at the DNA level that facilitate manipulations of modules (cf. Fig. 1 and Fig. S1) are described in detail in Supplementary Results.

Assembly of internal repeats

Three randomized internal repeats were PCR-assembled: the original DARPin I-repeat, the loop containing IL-repeat and the Asp1Ala-mutated IF-repeat, which follows the IL-repeat C-terminally in

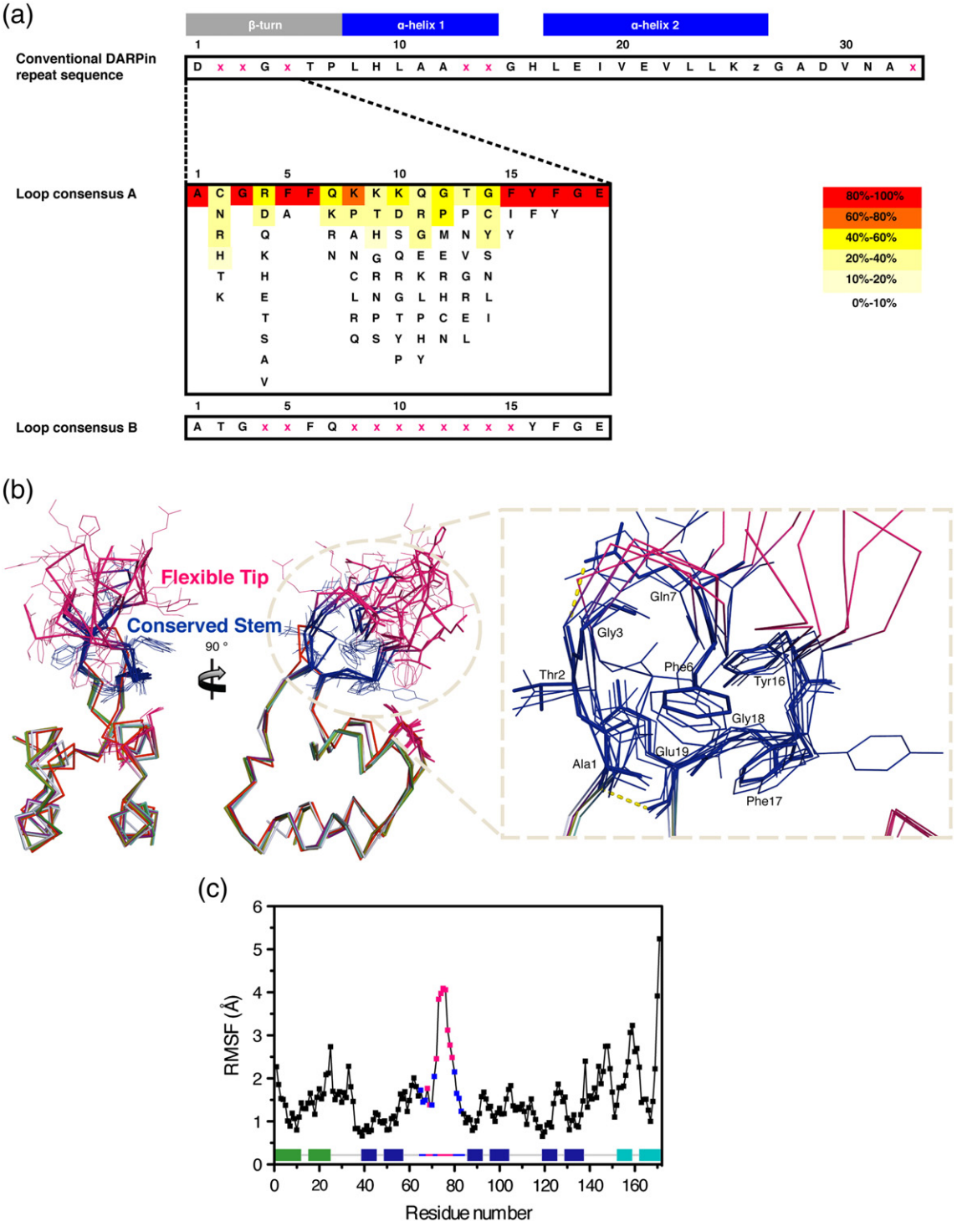

Fig. 3 (*legend on next page*)

the full-length LoopDARPin (Fig. 1 and Fig. S2); 72% (31 of 43 sequences) of I-repeats, 75% (36 of 48 sequences) of IL-repeats and 87% (41 of 47 sequences) of IF-repeats were devoid of deleterious frameshift mutations or stop codons.

Assembly of capping repeats

Unrandomized capping repeats were PCR assembled (N-cap: simply termed "N" and a stabilized C-cap version: "C" [63]) and subsequently used to create a first LoopDARPin library with unrandomized caps. Additionally, randomized versions of capping repeats (N-cap: termed N_{ran} and C-cap: C_{ran}) were assembled to be included in a cap-randomized LoopDARPin library.

To introduce a maximum level of variance with regard to the capping repeats, we mixed unrandomized and randomized capping repeats for the creation of our second LoopDARPin library. In this LoopDARPin library containing a cap mixture, the selection of the best combination of capping and internal repeats would be left to the *in vitro* selection system. After all, it might be possible that the additional variability in the caps might be somewhat detrimental for some sequences and thus be selected against. Therefore, randomized versions of capping repeats (N-cap: N_{ran} and C-cap: C_{ran}) and a modified version of the previously described C-capping repeat present in the original DARPin library (C_{old}) [7,63] were PCR assembled and mixed with unrandomized capping repeats N and C to yield a N-cap library mixture (N_{mix}) and a C-cap library mixture (C_{mix}) (see Supplementary Results for more details).

Assembly of full-length ribosome-display format LoopDARPin libraries

For ribosome-display selections, the naïve LoopDARPin library requires additional flanking sequence features present in the pRDV ribosome-display vector, such as the promoter and Shine–Dalgarno sequence upstream, and the tether and RNA hairpin downstream [42,64]. We created two separate capping-repeat-containing pRDV vectors. pRDV1 contained unrandomized caps N and C, whereas pRDV3 contained N_{mix} and C_{mix}. With this strategy, the generic fusion of either unrandomized or randomized caps to our core LoopDARPin library was possible in a single step (Fig. S2); for more details, see Supplementary Results. From the estimated number of molecules after each ligation step, the practical library size of both libraries was approximately 10^{11}.

Theoretical diversities of single repeats were N_{ran}-repeat $17^2 = 2.9 \times 10^2$, I-repeat $17^6 = 2.4 \times 10^7$, IL-repeat $17^3 \times 18^{10} = 1.8 \times 10^{16}$, IF-repeat $17^6 = 2.4 \times 10^7$ and C_{ran}-repeat $17^5 = 1.4 \times 10^6$. We denote the domain composition of the LoopDARPin library with three internal repeats as N-I-IL-IF-C (for nonrandomized caps) or LD_N3C for short, and we denote the one with randomized caps as N_{mix}-I-IL-IF-C_{mix} or LD_N_{mix}3C_{mix} for short. LoopDARPin libraries thus have a theoretical diversity of 1×10^{31}

Fig. 3. (a) Stepwise definition of the loop consensus used in the present study. For orientation, the secondary structure elements are indicated above the sequences. Loop consensus A was derived from an alignment of 86 natural ARs derived from a BLAST search against GenBank with the initially identified loop-containing natural ankyrin repeat protein of the N-terminal intracellular domain of the transient receptor potential (TRP) channel of the vanilloid receptor subfamily 2 (TRPV2) (PDB ID: 2F37). The amino acid conservation color code is indicated in the panel. Structure-based considerations (see Results) led from loop consensus A to loop consensus B, the final sequence of the loop consensus. In loop consensus B, the potential target interaction residues, which were randomized in the subsequent loop library, are indicated by a pink x. (b) Shown is the helix1-helix2-turn-helix1-helix2 search motif structure of the conventional DARPin (PDB ID: 2XEE, orange), structurally aligned with all lead structures, resulting in loop consensus B. All available helix1-helix2-turn-helix1-helix2 motif structures of the conserved N-terminal intracellular domain of transient receptor potential (TRP) channels of the vanilloid receptor subfamilies (TRPV) are included. TRPV1 (2PNN, cyan), rat TRPV2 (structures from two crystal forms: 2ETB, light green, and 2ETC, olive), human TRPV2 (2F37, purple) and TRPV6 (2RFA, light blue) possess a conserved stem (colored blue) and a flexible tip (colored pink) at their elongated loops. Fixed stabilizing framework positions (blue) derived from these structures and included in loop consensus B are indicated in the magnified view in the box. Frontal and lateral views of the aligned structures illustrate that the inserted loops possess restricted conformational flexibility at their stem, contrasted by the sampling of a larger conformational space at the tip of the loop. The lateral view shows that the loops fold somewhat over helix1, making these loop insertions perfectly suitable for the combination with additional interaction residues present in adjacent β-turns and within helix1 of loop-containing and neighboring repeats. This figure was created using PyMOL[¶]. (c) Molecular dynamics simulations for 50 ns at 300 K using the GROMOS 45A4 force field were applied to examine the flexibility of the consensus LoopDARPin. The RMSF around the average structure is shown. The overall mobility of the consensus LoopDARPin is low. The most flexible regions are located at the C-terminus and at the tip of the loop. Importantly, the stability at the stem of the loop is retained and permits the tip of the loop to sample a vast conformational space. Coloring is as in (b) with fixed framework positions colored blue and the subsequently randomized positions colored pink. Helices of the N-terminal capping repeat, the internal repeat modules and the C-terminal capping repeat are indicated by rectangular boxes and are colored as in Fig. 1 in green, blue and cyan, respectively.

and 4.2×10^{39}, respectively, vastly exceeding the practical diversity of all display systems. To assess the quality of the assembled LD_N3C and LD_$N_{mix}3C_{mix}$ LoopDARPin libraries on the DNA level, we sequenced single library members. DNA sequencing revealed that 7 of 18 (39%) LD_N3C and 23 of 66 (35%) LD_$N_{mix}3C_{mix}$ LoopDARPins possessed no frameshift, no stop codon but correct framework residues and correct trinucleotide codons. Observed results compared well to library qualities

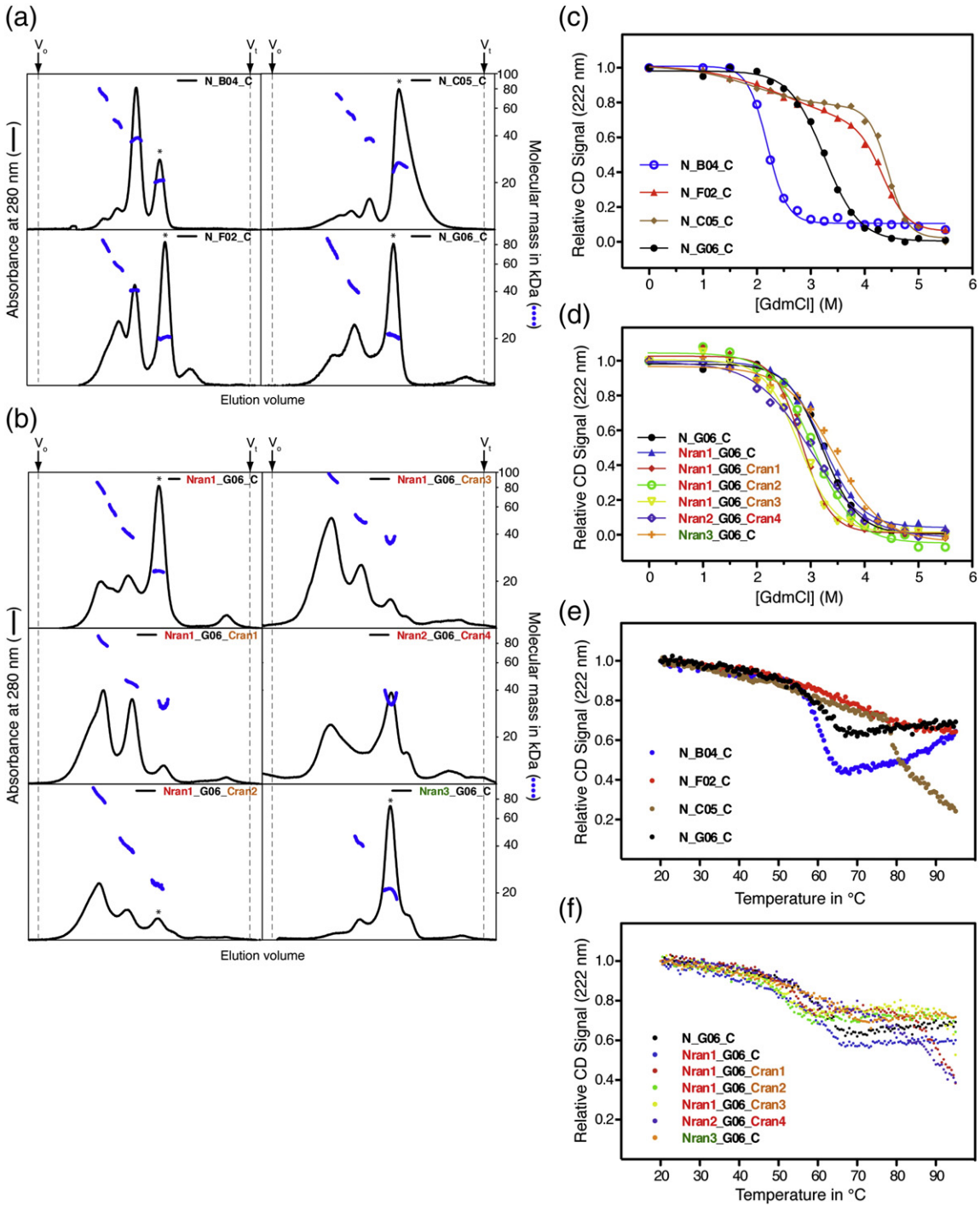

Fig. 4 (*legend on next page*)

obtained for earlier libraries [7,65]. A detailed sequence analysis of unselected library members is included in Supplementary Results.

Biophysical characterization of randomly chosen unselected library members

We performed in-depth biophysical analyses of 10 unselected library members to validate both our LoopDARPin design and our cap randomization strategy. Four unselected LoopDARPins with unrandomized caps (N_B04_C, N_C05_C, N_F02_C and N_G06_C) were analyzed in detail. For clarification of the nomenclature, N_G06_C, for example, is a LoopDARPin containing unrandomized N- and C-caps. To determine the influence of cap randomization on the biophysical properties of LoopDARPins, we also equipped N_G06_C with different randomized cap combinations. The G06 core was combined with three different randomized N-capping repeats ($N_{ran}1$ through $N_{ran}3$) and with four different C-capping repeats ($C_{ran}1$ through $C_{ran}4$). The biophysical properties of the resulting six G06 variants were compared to the original N_G06_C LoopDARPin. Relevant sequence positions of LoopDARPins characterized in detail are summarized in Fig. S3.

The mentioned LoopDARPins could all be expressed in soluble form in large amounts in *E. coli*. Expression of all LoopDARPins at 37 °C yielded 100–200 mg/l of soluble protein in shake flasks. The addition of randomized capping repeats to the G06 core did not affect expression yields (data not shown). Single-step immobilized metal-ion affinity chromatography (IMAC) yielded pure protein (data not shown). The molecular mass of the proteins was confirmed by mass spectrometry. LoopDARPins remained soluble and did not aggregate over weeks at 4 °C at a concentration of 10 mg/ml in TBS_{150} (pH 8.0).

Size-exclusion chromatography (SEC) coupled to multi-angle light scattering (MALS) revealed that two out of four LoopDARPins with unrandomized caps (N_C05_C and N_G06_C) are mainly monomeric at a concentration of 1 mg/ml (50 μM). Nonetheless, the chromatograms of both LoopDARPins possess small additional peaks at smaller retention volumes identified as the dimeric, trimeric and tetrameric species. For N_B04_C and N_F02_C, these species are more pronounced (Fig. 4a and Table 1).

Changing the unrandomized N- or C-capping repeat of N_G06_C to randomized capping repeat versions increased the overall dimer or oligomer formation tendencies. Figure 4b shows that the exchange of the overall hydrophilic unrandomized N-cap positions Arg11 and Ala12 of N_G06_C to the overall more hydrophobic randomized N-cap positions Trp11 and Gln12 in $N_{ran}1$_G06_C slightly increases oligomerization. However, exchanging these positions to hydrophilic randomized N-cap positions Lys11 and Glu12 in $N_{ran}3$_G06_C improves the monomeric behavior compared to the original N_G06_C LoopDARPin. Conversely, the exchange of the original unrandomized C-cap in $N_{ran}1$_G06_C to more hydrophobic C-caps increases oligomerization tendencies (Fig. 4b). The combination of N- and C-cap randomization, therefore, seems to reduce monomeric species of LoopDARPins, as hydrophobic residues are found more frequently. Analytical SEC experiments with increasing concentrations (5, 10, 20, 50 and 100 μM) of LoopDARPin showed that the

Fig. 4. (a and b) The monomeric or oligomeric state of 10 unselected LoopDARPin library members was analyzed by SEC, coupled to MALS. For sequence information, see Fig. S3. The elution profiles represent the absorption at 280 nm (left-hand *y*-axis). Indicated by a line of blue dots across the eluting peaks, the right-hand *y*-axis shows the molecular mass of the eluting particles as determined by MALS. (a) LoopDARPins with unrandomized caps. Two (N_C05_C and N_G06_C) out of four proteins are mainly monomeric at a concentration of 1 mg/ml (50 μM), whereas N_B04_C and N_F02_C possess significant additional dimeric, trimeric and tetrameric species. (b) The LoopDARPin N_G06_C was used to determine the influence of cap randomization on the protein assuming a monomeric or oligomeric state. The original unrandomized caps of N_G06_C were exchanged with randomized caps. A green, orange and red color in the name indicates that the added cap is more hydrophilic, more hydrophobic or significantly more hydrophobic than the original unrandomized cap, respectively. Overall dimerization and oligomerization tendencies increase with the addition of hydrophobic and very hydrophobic N- or C-caps, while addition of a hydrophilic cap reduces oligomerization tendencies. (c and d) Equilibrium unfolding of the 10 randomly chosen unselected LoopDARPin library members also investigated in (a) and (b). (c) LoopDARPins with unrandomized caps. (d) LoopDARPin G06 variants with different randomized caps. The equilibrium denaturation was followed by observing the CD signal at 222 nm (see Materials and Methods). The CD signal is displayed as fraction of the CD value of each sample at 0 M GdmCl. The unfolding of the LoopDARPins tested in the present study cannot be precisely described by a simple two- or three-state equilibrium system, and thus, no ΔG values are reported and the apparent midpoints of denaturation are summarized in Table 1. (e and f) Thermal denaturation of the 10 randomly chosen unselected LoopDARPin library members also investigated in (a) to (d). (e) LoopDARPins with unrandomized caps. (f) LoopDARPin G06 variants with different randomized caps. The denaturation was monitored by observing the CD signal at 222 nm (see Materials and Methods). The CD signal is displayed as fraction of the CD value of each sample at 20 °C. Due to aggregation, occasionally, an increase of the relative CD signal after denaturation was observed. The heating gradient was 1 °C/min and melting was only partially reversible [e.g., only 50% of the signal was regained upon cooling (data not shown)].

Table 1. Biophysical data of characterized LoopDARPins

Protein	CD_{222} (MRE)[a]	MW_{calc} (kDa)[b]	MW_{obs} (kDa)[c]	T_{m1} (°C)[e]	T_{m2} (°C)[e]	D_{m1} (M)	D_{m2} (M)[f]
N_B04_C	−12,645	19.8	20.8	59			2.19 ± 0.02
N_F02_C	−11,231	19.6	20.5	55	>95	2.57 ± 0.17[g]	4.33 ± 0.01[g]
N_C05_C	−9,102	19.9	26.4	55	>75	1.96 ± 0.29[g]	4.43 ± 0.01[g]
N_G06_C	−10,462	19.7	20.7	57	>95		3.24 ± 0.01
$N_{ran}1$_G06_C	−10,909	19.8	23.2	54	>95		3.25 ± 0.01
$N_{ran}1$_G06_$C_{ran}1$	−11,911	19.8	31.7[d]	53	>85		2.86 ± 0.02
$N_{ran}1$_G06_$C_{ran}2$	−7,068	19.8	22.3	49	>95		3.07 ± 0.01
$N_{ran}1$_G06_$C_{ran}3$	−12,879	19.7	35.6[d]	49	>90		2.82 ± 0.02
$N_{ran}2$_G06_$C_{ran}4$	−10,354	19.9	32.9[d]	55	>95		3.09 ± 0.01
$N_{ran}3$_G06_C	−13,500	19.7	21.0	55	>95		3.44 ± 0.02
008_H10	−10,127	19.5	22.9	63	>95		3.44 ± 0.02
008_C6	−14,451	19.7	19.9	65	>95		3.09 ± 0.01
001_C10	−11,746	19.5	21.3	57	>95		2.86 ± 0.01

[a] Mean residue ellipticity (deg cm^2/dmol) at 222 nm.
[b] MW (molecular mass) as calculated from the sequence.
[c] MW of monomeric species determined by SEC-MALS.
[d] MW of dimeric species determined by SEC-MALS.
[e] As determined by thermal unfolding observing the CD signal at 222 nm.
[f] Midpoint of denaturation as determined by GdmCl-induced unfolding observing the CD signal at 222 nm and assuming a two-state unfolding equilibrium [63,66].
[g] Midpoint of denaturation as determined by GdmCl-induced unfolding observing the CD signal at 222 nm and assuming a sequential three-state model [63,67].

observed oligomerization is concentration dependent (Fig. S4). Re-injection of collected monomer and oligomer fractions yielded the original chromatogram, which shows that oligomers can be reversibly transformed back into monomers (Fig. S5) upon dilution. This constitutes one of several arguments (see below) that the oligomer formation observed is the reversible association between folded monomers.

The CD spectra of all IMAC-purified LoopDARPins superimpose well with the spectrum of conventional DARPins, confirming that the secondary structure composition of LoopDARPins and conventional DARPins are the same (Fig. S6). The contribution of the additional amino acids from the loop is too small to affect the overall spectrum.

GdmCl equilibrium unfolding experiments of unselected library members show midpoints of unfolding between 2.25 and 4.5 M GdmCl (Fig. 4c and d and Table 1), which compares well to values determined for conventional DARPins (N3C DARPins: between 2.88 and 4.95 M GdmCl) [12]. Most LoopDARPins tested here show a single cooperative transition. However, the more stable LoopDARPins N_F02_C and N_C05_C possess a "pretransition" at 2.5 M GdmCl, before the main transition, which occurs at 4.25 M GdmCl. The denaturation of these LoopDARPins may thus involve an intermediate. A similar behavior with an intermediate state has previously been described for very stable conventional DARPin variants [63], where the equilibrium intermediate was identified as a state where the C-terminal capping repeat was selectively denatured. In that study, it was found that the first transition, causing the loss of about 20% of the initial helical CD signal, originated from the selective unfolding of the C-cap, whereas the main transition involved the unfolding of all other repeats. In variants with more stable internal repeats showing this effect, the unfolding of the C-cap is uncoupled, giving rise to the observed equilibrium intermediate, with the C-terminal capping repeat detached from the central repeats still intact.

Since we also observe for our most stable LoopDARPins this pretransition, where the initial helical CD signal is decreased by about 20%, it might be possible that our apparent unfolding intermediate also corresponds to a LoopDARPin, where the C-cap (one out of the total five repeats) is selectively unfolded (Fig. 4c). If this were the case, very stable LoopDARPins would inherit the uncoupled unfolding of the C-cap from very stable conventional DARPins. An alternative cause for the observed pretransition could be the partial unfolding of the loop-containing internal repeat of the LoopDARPin. Unfolding of an internal repeat, however, would lead to the destabilization of adjacent repeats both N- and C-terminally and would therefore drastically decrease the stability of the entire LoopDARPin. We hypothesize that such a destabilization would lead to a complete and not only to a partial unfolding of the protein. In addition, the pretransition could also be caused by the selective unfolding of the N-cap. Further experiments are necessary to discriminate between the described possibilities. Since most denaturation curves are not well described by two-state equilibria, we do not report any ΔG values.

Thermal stability of the 10 described randomly chosen unselected library members was determined through measuring the CD signal at 222 nm upon heat denaturation (Fig. 4e and f and Table 1). As for

conventional DARPins, heat denaturation was only partly reversible (data not shown). With respect to thermal unfolding, all LoopDARPins tested can be divided into four groups: (i) the least stable LoopDARPin tested shows a single transition at 60 °C (e.g., N_B04_C). (ii) The more stable LoopDARPins possess two transitions and denature via an apparent intermediate. They share the first transition at 50–60 °C with the least stable LoopDARPin but posses a main transition above 80–90 °C (e.g., $N_{ran}1\_G06\_C_{ran}1$, $N_{ran}1\_G06\_C_{ran}3$ and $N_{ran}2\_G06\_C_{ran}4$). (iii) A third group of LoopDARPins only shows the first transition at 50–60 °C but cannot be denatured further (e.g., N_G06_C, $N_{ran}1\_G06\_C$, $N_{ran}1\_G06\_C_{ran}2$ and $N_{ran}3\_G06\_C$). (iv) LoopDARPins not falling into any of the other groups are N_F02_C and N_C05_C, and these two are the most stable LoopDARPins tested by GdmCl-induced unfolding. N_F02_C shows no temperature-induced transition and retains significant secondary structure even after heating the sample to 95 °C. N_C05_C does not show a first transition at 50–60 °C, but it seems to largely unfold above 80–90 °C. Additional experiments will be necessary to characterize the observed unfolding intermediates. Importantly, with midpoints of unfolding between 50 and more than 95 °C, LoopDARPins share the considerable heat resistance of conventional DARPins [7].

Cap randomization has no negative influence on stability (Fig. 4d and f). Stabilities of cap-randomized G06 LoopDARPin variants are very similar to the stability of LoopDARPin N_G06_C with unrandomized caps. $N_{ran}1\_G06\_C$ and $N_{ran}3\_G06\_C$ with midpoints of denaturation of 3.25 and 3.44 M GdmCl, respectively, are slightly more stable than N_G06_C with a midpoint of denaturation of 3.24 M GdmCl. The remaining four cap-randomized G06 LoopDARPin variants show a slight reduction in stability with midpoints of denaturation between 2.82 and 3.09 M GdmCl.

No concentration dependence of stability to GdmCl or heat was observed, as curves did not change with concentration (data not shown). This suggests that, even though some of the LoopDARPins do form reversible oligomers, these forms have no measurable influence on stability.

Importantly, the high degree of stability of DARPins is retained in LoopDARPins, underlining the success of our design. However, the dimerization and oligomerization tendency of LoopDARPins is higher than for conventional DARPins, as judged by SEC-MALS. Seven out of ten LoopDARPins possess considerable dimeric or oligomeric species (Fig. 4a and b), which can be addressed by further engineering (see below). In contrast, only one out of six original DARPins without loop and without randomized caps showed dimerization tendencies [7].

From the given results from stability and secondary structure determinations and supported through the structure of $N_{ran}1\_G06\_C$ (see the next section), we conclude that this dimerization and oligomerization tendency (seen for this LoopDARPin in Fig. 4b) is not caused by the unfolding of LoopDARPins but, rather, through self-complementarity of their extended hydrophobic surface facilitated by the increased conformational flexibility of the loop. An additional observation supports this hypothesis: two $N_{ran}1\_G06\_C$ LoopDARPins with very distinct loop conformations are present in the asymmetric unit of our crystal structure. Contacts between the two molecules are largely made through self-complementary loop and cap interactions (Fig. 5b), thus very directly illustrating this concept.

We therefore conclude that reversible dimerization and oligomerization of LoopDARPins is governed by low-affinity interactions between folded molecules. Nonetheless, the self-complementarity of LoopDARPins can almost certainly be optimized through further engineering, without compromising the advantageous properties of the LoopDARPins. As we were able to select highly specific, high-affinity LoopDARPins at unparalleled speed against several target proteins (see below), we believe that we found a workable balance between self-complementarity and the ability to provide a hydrophobic interaction surface needed for very high affinity binding, which can further be fine-tuned.

Crystallographic LoopDARPin design validation: Crystal structure of $N_{ran}1\_G06\_C$

The crystal structure of $N_{ran}1\_G06\_C$ was solved to a resolution of 1.7 Å (Table ST1). Two molecules are present in the asymmetric unit, packing face-to-face involving their target binding surfaces in an antiparallel orientation. Clear electron density extends from Asp13 to Ala182 and from Asp13 to Ala183 for the first and second molecule, respectively. The N-terminal $MRGSHis_6$ tag residues are flexible and therefore not visible in the electron density of either molecule.

The presented high-resolution structure of a LoopDARPin allows us to validate the success of the four main features of our LoopDARPin design (Fig. 5).

(i) Superimposition of the X-ray structure of LoopDARPin $N_{ran}1\_G06\_C$ and conventional DARPin 2XEE shows that their framework positions are practically identical. LoopDARPin molecule 1 and the conventional DARPin possess an RMSD C^{α} of all non-loop positions of only 0.58 Å. Thus, the insertion of our designed loop into the existing DARPin scaffold does not alter the structure of the DARPin framework.

(ii) The two LoopDARPins in the asymmetric unit adopt two different loop and IF-β-turn

conformations, thus validating the designed conformational flexibility at these positions. In both structures, the stem of the loop serves as a stabilizing basis for the conformationally flexible tip of the loop.

(iii) Randomization of the N-terminal capping repeat does not alter the repeat structure.
(iv) Over 45% of all randomized positions contribute to the face-to-face packing and 40% of these interacting positions are randomized

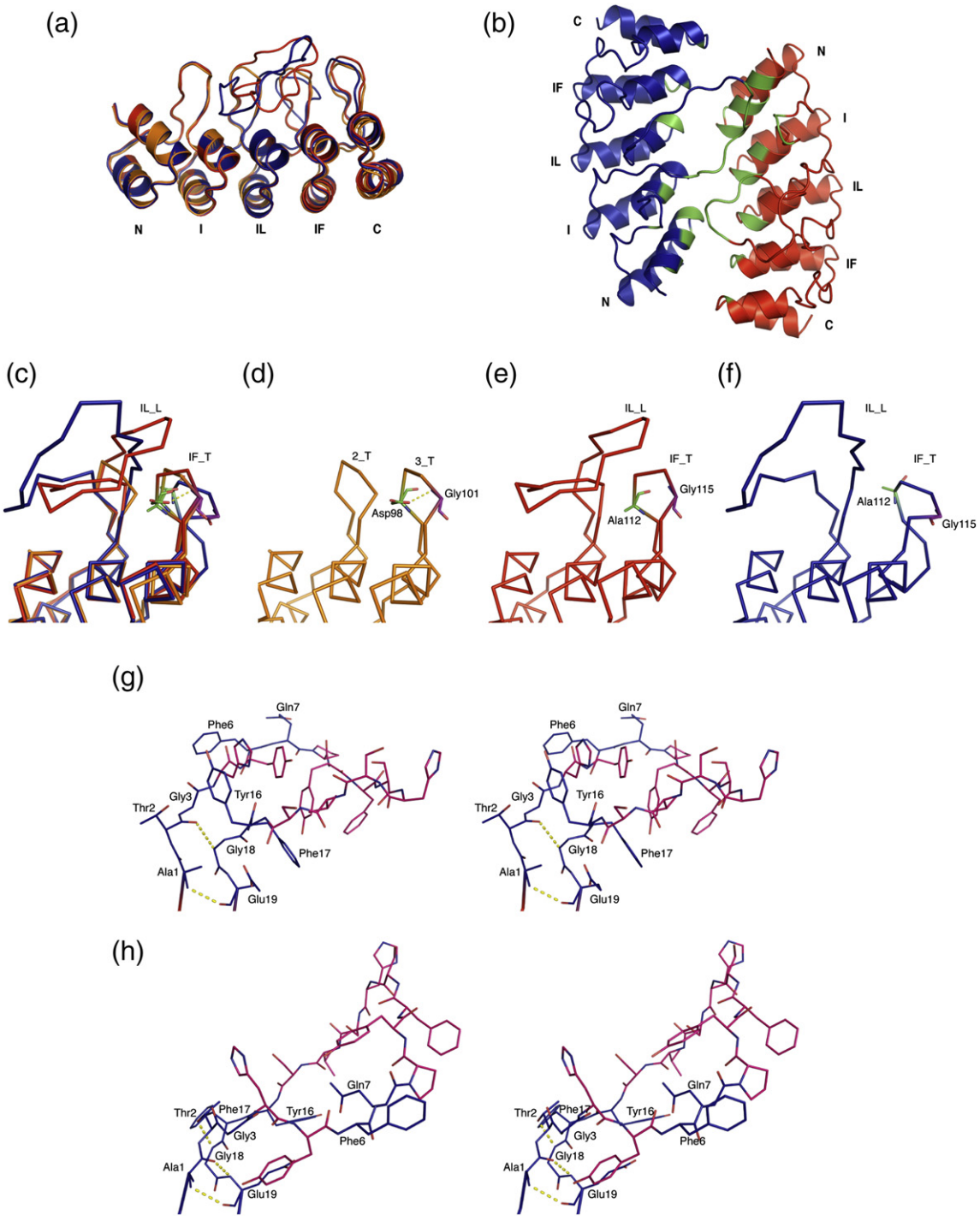

Fig. 5 (*legend on next page*)

loop positions. All randomized N-cap positions are involved in forming the interface, and the unrandomized C-cap is largely excluded from this interface, underlining that both loop and cap randomization contribute to a continuous interaction surface.

Stem positions in LoopDARPin design and structure: Consistencies and deviations

Stem positions Ala1, Thr2, Gly3, Tyr16, Phe17, Gly18 and Glu19 fulfill their intended function in maintaining the stem conformation of the loop (Fig. 5). Tyr16 and Phe17 are not at the exact intended positions and their location in molecules 1 and 2 differ, but they perfectly execute their designed function of stabilizing the hydrophobic core of the loop. Both Gly3 and Gly18 serve as flexible linking residues as planned, which help to thread the flexible loop back into the DARPin framework. Both in molecules 1 and 2, Gly18-NH is involved in a stabilizing H-bond with either Thr2-CO (molecule 1) or Thr2-OH (molecule 2). Although these interactions were not intended by the design, the close proximity of Thr2 and Gly18, combined with the flexibility of Gly18, allows different stabilizing H-bond combinations. Ala1-NH and Glu19-CO are connected through an H-bond, as designed. In case of molecule 2, a second H-bond between Ala1-CO and Glu19-NH further stabilizes the core structure of the loop. The presented structure confirms that we succeeded in designing an interaction network rich in H-bonds and hydrophobic interactions, combined with the necessary degree of flexibility at linking positions.

The framework loop positions of Phe6 and Gln7 are not present at locations intended by the design. Phe6 was conserved both in sequence and in structure, whereas position 7 was only conserved structurally in natural ankyrin repeats containing such a loop. Both positions are surrounded by randomized positions (Fig. 3). Analyzing the N_{ran}1_G06_C structure, it seems that the hydrophobic interaction between Phe6 and Ala1 and the H-bond between the Gln7 side chain and the Thr2 backbone in the designed structure cannot be maintained with altered randomized loop positions. Nevertheless, the structural integrity of the loop is not affected by these missing interactions. Both residues point to the backside of the LoopDARPin in molecule 1. In molecule 2, however, they point toward a potential target (Fig. 5g and h). By design, framework positions should not interfere with target binding. Due to the intended conformational flexibility of the loop, positions further away from the stem of the loop are more difficult to design and should therefore be randomized in future iterations to allow more structural adaptation.

Conformational flexibility in the IF-β-turn

The loop conformation in molecule 1 leaves the following IF-β-turn unchanged (Fig. 5c–f). However, in molecule 2, the loop adopts a different conformation and forces the IF-β-turn region to partially fold away from the loop. The structural integrity outside the β-turn is unaltered. The new β-turn conformation leads to a rearrangement of the randomized positions, offering an adjusted target interaction surface. Such a flexibility on demand was included in the LoopDARPin design by disrupting the original H-bond network. The

Fig. 5. (a and b) Crystal structure of N_{ran}1_G06_C. (a) Superimposition of the X-ray structure of LoopDARPin N_{ran}1_G06_C (molecules 1 and 2 present in the asymmetric unit are colored red and blue, respectively) and conventional DARPin 2XEE (colored orange). The positions of framework residues of LoopDARPin and conventional DARPin are practically identical. Different conformations of the inserted loop in the LoopDARPin are compatible with the repeat protein structure, and randomization of the N-terminal capping repeat does not alter the repeat structure. (b) Representation of the asymmetric unit. The C^{α} atom of contact residues within 3 Å of each other is highlighted in green. Most randomized positions, especially from the loop and the randomized N-cap, contribute to the face-to-face packing, whereas the unrandomized C-cap is practically excluded from the interface. N, N-cap; I, internal repeat; IL, loop-containing internal repeat; IF, loop-following internal repeat; C, C-cap. The figure was prepared with PyMOL[¶]. (c–f) Designed conformational flexibility of loop and IF-β-turn in LoopDARPins confirmed by crystal structure of N_{ran}1_G06_C. Nomenclature as in Fig. 1. Coloring as (a) and (b). Only the second and third internal repeats of the X-ray structure of LoopDARPin N_{ran}1_G06_C molecules 1 and 2 and conventional DARPin 2XEE are shown. (c) Superimposition of LoopDARPin N_{ran}1_G06_C molecules 1 and 2 and conventional DARPin 2XEE. (d) Conventional DARPin 2XEE with stabilizing β-turn H-bond interaction between Asp98 side chain and Gly101 amide nitrogen (shown as broken line). (e) LoopDARPin N_{ran}1_G06_C molecule 1. The stabilizing IF-β-turn H-bond interaction present in conventional DARPins has been removed by removing the Asp side chain to introduce flexibility. (f) LoopDARPin N_{ran}1_G06_C molecule 2. The loop adopts a different conformation than in molecule 1, thus utilizing the flexibility in the adjacent IF-β-turn. Note that although the IF-β-turn region partially folds away from the loop, the structural integrity outside the β-turn is unaltered. (g and h) Stereo view of crystal structure of the loop region in N_{ran}1_G06_C molecule 1 (g) and molecule 2 (h). Fixed stabilizing framework positions (blue) are highlighted. The flexible randomized tip of the loop is colored pink. The loop in LoopDARPin N_{ran}1_G06_C possesses, as intended by design, a high degree of flexibility. The designed H-bonding network together with stabilizing hydrophobic interactions at the stem of the loop enables the loop in N_{ran}1_G06_C molecules 1 and 2 to adopt completely different conformations in their tip region.

presented structure exemplifies the benefits of this design feature.

Structure of a randomized N-cap

Changing original N-cap framework positions Arg11 and Ala12 to Trp11 and Gln12, both a result of randomization, maintains the correct fold of the N-terminal capping repeat. In fact, the RMSD C^{α} of the N-cap between both LoopDARPin structures and the conventional DARPin N-cap is less than 0.3 Å (Fig. 5a). Since the stability of G06 with unrandomized or randomized caps is largely identical (Fig. 4c–f and Table 1), the available structure underlines that cap randomization can be employed to further increase the continuous interaction surface of LoopDARPins.

Target selection and expression: ERK2 and BCL-2 family members

To test the performance of LoopDARPins in rapidly selecting high-affinity binders against multiple target proteins, we chose the pro-proliferative kinase ERK2 and four members of the BCL-2 family (BCL-2, BCL-XL, BCL-W and MCL-1) of anti-apoptotic regulators as the first target proteins for evaluating our libraries (Fig. 2). These proteins are often involved in the development of cancer. The selection of high-affinity binders would therefore open up new possibilities to further investigate the role and function of these proteins [21,68] and could serve as a starting point for the development of future drugs.

ERK2 is a member of the mitogen-activated protein kinase family. As evolutionarily conserved serine/threonine kinases, they are activated in response to extracellular stimuli and mediate signal transduction from the cell surface to the nucleus. Mitogen-activated protein kinases regulate several physiological and pathological processes, including inflammation, apoptosis, oncogenic transformation and metastasis [69]. ERK2 is a well-characterized eukaryotic kinase [70], which can be readily expressed in *E. coli* and purified. Previously, several conventional DARPins binding to ERK2 with a nanomolar K_D and distinguishing the phosphorylated (active) and non-phosphorylated (inactive form) had been selected [21,68].

As a second series of targets, a family of proteins, the anti-apoptotic members of the BCL-2 family (Fig. 6), were chosen as the main targets for the evaluation of our LoopDARPin design. A structure-based sequence alignment of the anti-apoptotic BCL-2 family members (BCL-2, BCL-XL, BCL-W and MCL-1) used in the present study is shown in Fig. S7. This central protein family regulates apoptosis, a process essential for development and tissue turnover, and perturbation of this process leads to diseases ranging from autoimmune disorders to cancer [76–79]. A key feature of anti-apoptotic BCL-2 family members is their conserved, surface-exposed hydrophobic groove (Fig. 6). With this groove, they interact with the pro-apoptotic BH3-only proteins (e.g., BIM) and inhibit their ability to drive apoptosis [76,80–82]. Not surprisingly, enhanced expression of anti-apoptotic BCL-2 family members is found in many cancers [83–89].

Therefore, anti-apoptotic BCL-2 family members have attracted significant attention as therapeutic targets and, predominantly, small molecule inhibitors with sometimes still elusive mechanisms of cell killing [90,91] and varying degrees of specificity and effectiveness have been developed [92–102]. The availability of specific high-affinity inhibitors for functional cellular assays or future therapy is therefore still very limited. Many inhibitors bind to the highly related proteins BCl-2, BCL-XL and BCL-W, but not to the more distantly related MCL-1, because they exclusively target the conserved hydrophobic groove of the anti-apoptotic BCL-2 family members. As a consequence, MCL-1 up-regulation is a major source of

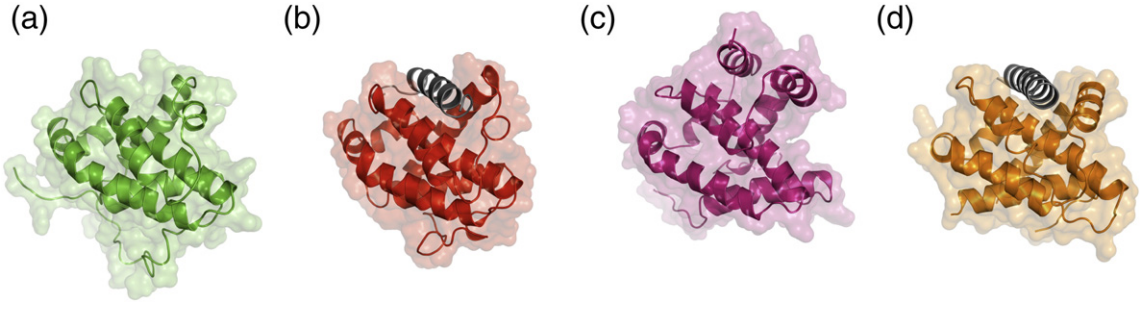

Fig. 6. Structures of the anti-apoptotic BCL-2 family members used in the present study. (a) BCL-2 (green) (PDB ID: 1G5M) [71]. (b) BCL-XL (red) in complex with the BECLIN peptide (gray) (PDB ID: 2PON) [72]. (c) BCL-W (pink) (PDB ID: 1MK3) [73]. (d) MCL-1 (orange) in complex with the BIM peptide (gray) (PDB ID: 2PQK) [74]. Anti-apoptotic BCL-2 family members possess very similar three-dimensional structures with two central hydrophobic α-helices surrounded by five amphipathic α-helices. Note that BCL-W possesses an additional helix (α8), which binds to its hydrophobic groove, but can be displaced by groove-binding ligands [75]. The figure was prepared with PyMOL[¶].

resistance to these compounds [103,104]. The capability to simultaneously target all anti-apoptotic BCL-2 family members would thus be beneficial.

We therefore aimed at selecting a set of LoopDARPins (Fig. 2), which block the groove-mediated interaction between anti-apoptotic BCL-2 family members and pro-apoptotic BH3-only proteins (Fig. 6). Such blocking of the groove region of either several family members simultaneously (pan-BCL-2 binders) or specific single family member would be both of great interest. We assumed that, with the large interaction surface provided by LoopDARPins, we could generate binders, which are able to provide additional contacts outside of the conserved regions in order to retain specificity, which is difficult to achieve with small molecule inhibitors.

Thus, all targets were produced both in biotinylated and in non-biotinylated forms. During ribosome-display selections, the biotinylated form of the targets was used in the panning step. Non-biotinylated target was used as competitor in later stages of all selections to increase selection pressure toward high affinity ("off-rate selection"). Since the natural BH3-only BIM peptide ligand binds to the surface-exposed hydrophobic groove of the anti-apoptotic BCL-2 family members, this interaction was used to confirm the functionality of the produced targets. In analytical SEC experiments, we observed a quantitative target/BIM complex formation supporting the correct folding of the produced BCL-2 family members (see Materials and Methods and Fig. S8).

Four-round ribosome-display selections against ERK2 using the N-I-IL-IF-C LoopDARPin library

First, we wanted to assess the quality of our LoopDARPin design using fixed caps. Thus, we performed initial ribosome-display [41,42] selections with biotinylated ERK2 bound to streptavidin-coated magnetic beads using the N-I-IL-IF-C (or LD_N3C for short) LoopDARPin library with unrandomized capping repeats (Figs. 1 and 2).

An initial measure for the successful recovery of binders during selections is the enrichment over background of reverse-transcribed recovered RNA after a ribosome-display round [42], typically seen only in later ribosome-display selection rounds. Surprisingly, such an enrichment of LoopDARPins was observed already after the first selection round. Stringency was therefore steadily increased during rounds two and three through elongated washing steps, and finally, an off-rate selection using a 250-fold excess of non-biotinylated competitor was included in the fourth round.

After this last ribosome-display selection round, 48 individual selected binders were screened by enzyme-linked immunosorbent assay (ELISA) using crude *E. coli* extracts to identify initial lead LoopDARPins. After four rounds of selection as described above, 5 of 48 assayed clones (10.4%) showed specific binding to ERK2 (signal/background $\geq$ 10). None of the analyzed LoopDARPins showed significant binding to microtiter plates coated with streptavidin and BSA (*b*ovine *s*erum *a*lbumin). These initial binders were sequenced and all sequences were found to be unique, in frame and containing no stop codons (data not shown). Further characterizations were conducted to assess the quality of the selected binders. The five initial LoopDARPin hits were purified using IMAC and further tested by analytical SEC for monomeric behavior. Out of five proteins, only LoopDARPin 4.3.E_E7 showed largely monomeric behavior, while the rest possessed a significant oligomeric fraction (data not shown). The sequence of 4.3.E_E7 is shown in Fig. S9.

The binding of 4.3.E_E7 to ERK2 was subsequently characterized in more detail. To investigate specificity, we performed ELISA experiments with the purified ERK2 binding LoopDARPin 4.3.E_E7 (Fig. 7). 4.3.E_E7 is specific for ERK2 and interacts neither with any of the BCL-2 family members (Fig. 7a) nor with streptavidin or BSA (Fig. 7b). In a competition ELISA experiment, the interaction of 4.3.E_E7 with immobilized ERK2 could be specifically inhibited by preincubation with non-biotinylated target (50% inhibition at 2.5 nM) (Fig. 7b). The affinity estimated from this experiment was consistent with surface plasmon resonance (SPR) measurements (see below). For comparison, the unselected LoopDARPin C05 did not interact with ERK2 or any BCL-2 family member, indicating that LoopDARPins per se do not bind to the mentioned targets (Fig. 7b). To determine the K_D of the interaction with its target ERK2, we analyzed LoopDARPin 4.3.E_E7 at multiple concentrations using SPR experiments (Table 2 and Fig. 7c). Using a global kinetic fit, we determined a K_D of 4.8 nM, serving as a first indication that the selection of specific high-affinity LoopDARPins within four rounds of ribosome-display selections is possible.

Three-round ribosome-display selections against BCL-2 family members using the N_{mix}-I-IL-IF-C_{mix} LoopDARPin library

We next tested the ability of our cap-randomized LoopDARPin library N_{mix}-I-IL-IF-C_{mix} (or LD_N_{mix}3C_{mix} for short) to generate specific high-affinity binders against a family of eukaryotic proteins (Fig. 2), the BCL-2 family (BCL-2, BCL-XL, BCL-W and MCL-1) of anti-apoptotic regulators (Fig. 6). Since the LD_N_{mix}3C_{mix} LoopDARPin library contains all combinations of N- and C-caps (N-C_{old}, N-C, N-C_{ran}, N_{ran}-C_{old}, N_{ran}-C, N_{ran}-C_{ran}), we assumed that this additional level of diversity together with the fact that LoopDARPins with randomized caps possess an increased continuous potential interaction surface would allow a very stringent selection approach. Thus, we conducted parallel selections with our

$LD\_N_{mix}3C_{mix}$ LoopDARPin library against the four BCL-2 family members BCL-2, BCL-XL, BCL-W and MCL-1, directly using the same stringency already in the first round that we had used in the second round in the selection against ERK2 (see Fig. 2 and Materials and Methods).

In order to select binders that are able to efficiently block the interaction between anti-apoptotic BCL-2 family members and pro-apoptotic BH3-only proteins, we included a prepanning step prior to each selection round (Fig. 2), using biotinylated target complexed with a BH3-only BIM peptide, fused to biotinylated protein D (pD). Since the BIM peptide binds into the surface-exposed groove of all BCL-2 family members with high affinity [107], only regions outside of the groove area would be accessible to the *in vitro* transcribed and translated LoopDARPin library during prepanning. With this prepanning step, LoopDARPin library members that bind outside of the groove region would therefore be removed. The remaining LoopDARPin library members should hence bind in the groove area and would be recovered in the following

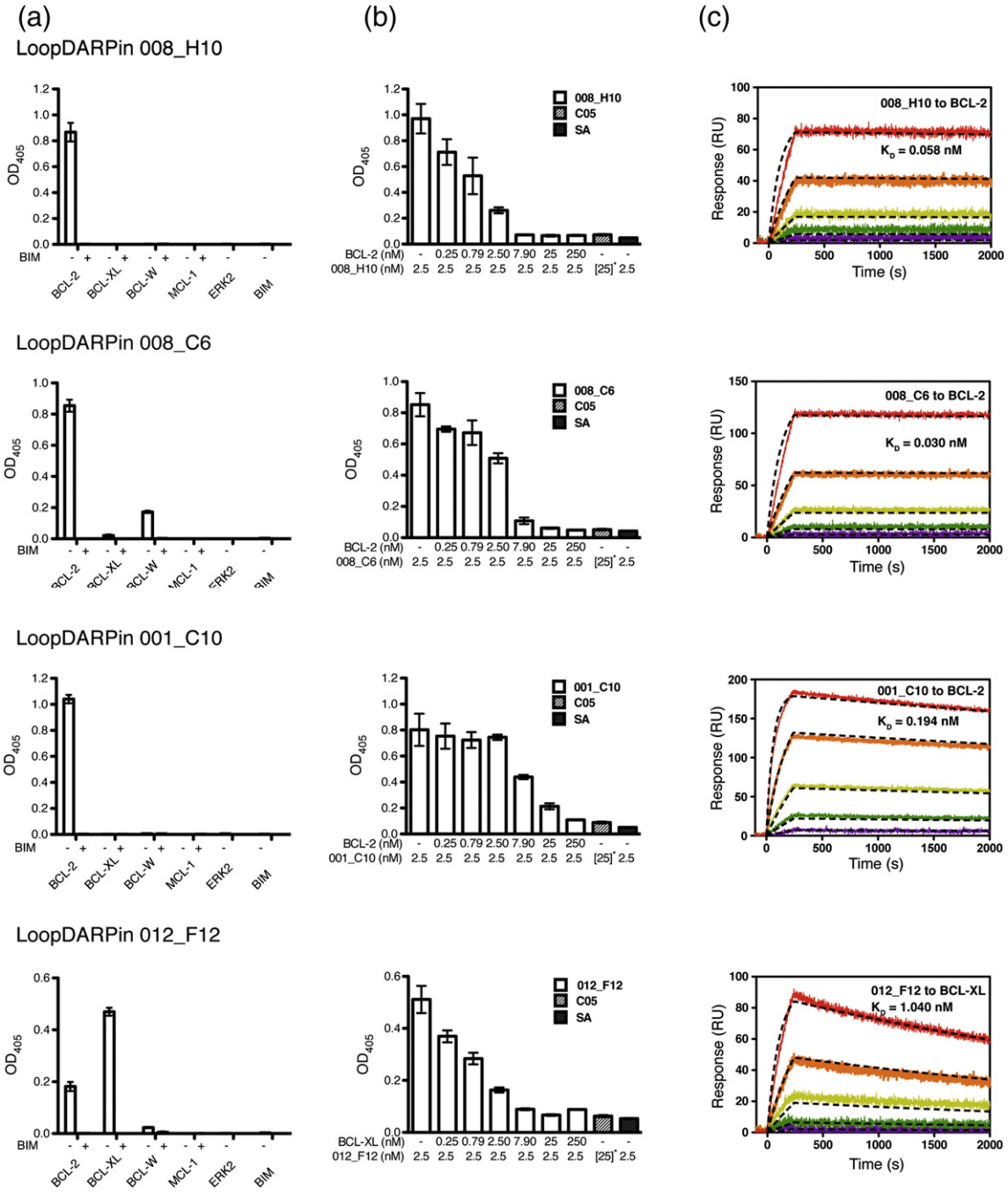

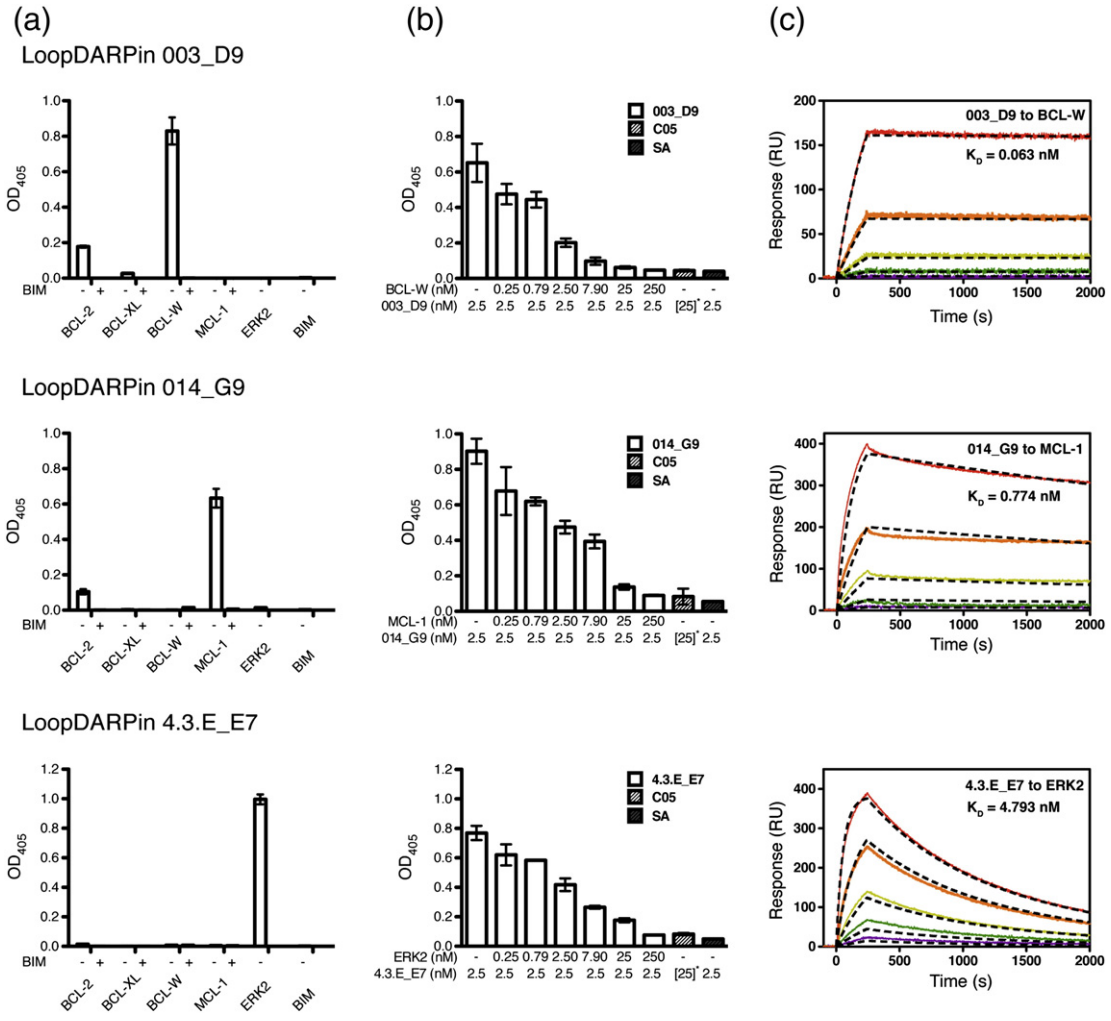

Fig. 7. Specificity and affinity of representative selected LoopDARPins for the target they were selected against. (a) Background-corrected ELISA signals to determine binder specificity. The interaction of all selected LoopDARPins (5 nM) with immobilized anti-apoptotic BCL-2 family members (– BIM) can be blocked by preincubation with a stoichiometric excess of the natural BIM peptide ligand (+ BIM), indicating that the groove-directing prepanning ribosome-display strategy worked out and that selected BCL-2 family binders bind into or near the surface-exposed groove. Direct interaction of binders with the BIM peptide does not occur (last column). Note that the background binding of LoopDARPins to the surface without immobilized target (<10% of total binding) has been subtracted. (b) Competition ELISA illustrating the interaction between binders and their original target. Binders (final concentration, 2.5 nM) were incubated with varying concentrations of free target before binding on immobilized target. Binding of all selected binders can be specifically inhibited by increasing concentrations of free target in solution. The unselected LoopDARPin C05 [hatched column, denoted with asterisk (*)] showed no interaction with any target at 25 nM, giving a signal identical with that of the control (SA [streptavidin only], 2.5 nM selected binder without immobilized target). (c) SPR analyses. Different concentrations of LoopDARPin (50, 15.81, 5, 1.58, 0.5 and 0 nM; red to gray) were injected simultaneously on parallel lanes during one run, followed by washing with buffer flow. The global fit is indicated by black broken lines (see Table 2 for the extracted kinetic data and legend to Fig. 8 and Supplementary Results for the used fitting model). Results for all selected binders are shown in Figs. S10 and S11.

panning step with uncomplexed target. Note that the interaction between BIM and the anti-apoptotic family members was also used to confirm the correct folding of the produced targets and for this reason, this interaction was also functionally verified by SEC (see Materials and Methods and Fig. S8).

Due to encouraging binder enrichment over background at the level of reverse-transcribed recovered RNA for all targets, the stringency was increased in round two and an off-rate selection using a 250-fold excess of non-biotinylated competitor was included in the third round.

Table 2. Kinetic binding data for a representative group of selected LoopDARPins determined by SPR

LoopDARPin	Target	k_{on} (M^{-1} s^{-1})	k_{off} (s^{-1})	K_D (M)
008_H10	BCL-2	2.03×10^5	1.17×10^{-5}	5.79×10^{-11}
008_C6	BCL-2	1.56×10^5	4.64×10^{-6}	2.97×10^{-11}
001_C10	BCL-2	3.40×10^5	6.60×10^{-5}	1.94×10^{-10}
012_F12	BCL-XL	1.90×10^5	1.97×10^{-4}	1.04×10^{-9}
003_D9	BCL-W	7.42×10^4	4.70×10^{-6}	6.33×10^{-11}
014_G9	MCL-1	1.59×10^5	1.23×10^{-4}	7.74×10^{-10}
4.3.E_E7	ERK2	1.75×10^5	1.04×10^{-3}	4.79×10^{-9}

To identify initial lead LoopDARPins, we screened 94 individual selected binders for each target selection by ELISA using crude *E. coli* extracts after the last round of this three-round ribosome-display selection. Depending on the target, varying numbers of binders showed specific binding (signal/background $\geq$ 10) to their target. Most binders were obtained from selections against BCL-2 and BCL-W [6 of 94 assayed clones (6.4%) and 7 of 94 assayed clones (7.4%), respectively]. Fewer binders were obtained from the selections against BCL-XL and MCL-1 [2 of 94 assayed clones, respectively, (2.1%)]. None of the analyzed LoopDARPins showed significant binding to microtiter plates coated with streptavidin and BSA. All initial binders were sequenced and their sequences were found to be unique, in frame and containing no stop codons (data not shown). Among selections with several initial leads, no identical clones were found, indicating that considerable diversity was still left in the selected pool and that stringency could still be further elevated.

Surprisingly, two binders from the BCL-W selection (013_H8 and 013_D12) had no loop (see Fig. S9). The two binders clearly originated from the LoopDARPin library, as they contained all the design features that had been included in the newly created LoopDARPin libraries on the nucleotide level, which were not present in the original DARPin library without loop. Therefore, the loop most likely had been deleted during PCR.

The applied selection pressure, with a prepanning on peptide–target complex (see above), forced binders to bind into the groove. After comparing surface shape and dimensions of the β-turns in conventional DARPins with the surface-exposed groove of BCL-W, we immediately recognized the perfect shape complementarity. Moreover, indeed, we now have structural data available for both complexes, which clearly show the perfect binding of both DARPins into the groove of BCL-W (J.S. and A.P., unpublished results). Interestingly, the K_D of the interaction between BCL-W and both loop-deleted binders 013_H8 and 013_D12 is 1 order and 2 orders of magnitude weaker than the interaction with the most affine LoopDARPin 003_D9 (see below).

All initial binders were IMAC purified and further screened by analytical SEC for monomeric behavior and for slowest off-rates by SPR. Three out of six BCL-2 binders, one out of two BCL-XL binders, four out of seven BCL-W and one out of two MCL-1 binders showed largely monomeric or dimeric behavior and slow off-rates, while the remaining binders possessed a significant oligomeric fraction or fast dissociation from the target (data not shown). For sequences of the final hits, see Fig. S9.

ELISA and SPR experiments were performed to determine the specificity and the K_D of all nine positive hits to the target that they were selected against and to the remaining family members, to get a quantitative measure of specificity. The results obtained for representative LoopDARPins from each target selection are shown in Table 2 and Fig. 7 (results for all binders are shown in Table ST2 and Figs. S10 and S11). The K_D matrix in Fig. 8 summarizes the K_D values determined by SPR for interactions between all targets and all LoopDARPins/DARPins. The binding of all selected LoopDARPins/DARPins to their biotinylated target could be blocked through the preincubation of the target with an excess of free pD-BIM, indicating that the prepanning strategy worked and that all LoopDARPin/DARPin hits indeed bind into or near the target groove (Fig. 7a and Fig. S10a).

Since sequence and structure homology among the used BCL-2 family members is very high [80] (Fig. 6 and Fig. S7) and since the applied selection strategy forced the selection toward binding to the groove but not to specific family members, it is not surprising that LoopDARPins/DARPins binding to more than one member of the family have been obtained. Nevertheless, also very specific binders have been selected (Figs. 7a and 8 and Figs. S10a and S11). Both types of binders are, of course, highly valuable tools for future applications.

LoopDARPins that bind with high affinity exclusively to the target they have been selected against (selectivity > 25 based on K_D values determined by SPR measurements) include 001_C1, 001_C10 (BCL-2 selection), 003_D9 (BCL-W selection) and 014_G9 (MCL-1 selection) (Fig. 8 and Fig. S11). The remaining LoopDARPins/DARPins bind measurably, but still weaker, to non-cognate family members as well. Strikingly, no binders selected against BCL-2, BCL-XL or BCL-W bind MCL-1. Similarly, none of the MCL-1 binding LoopDARPins interact with the other family members, highlighting the structural differences between MCL-1 and the other family members [74]. Specificities determined by ELISA are consistent with SPR measurements (Fig. 7a/Fig. S10a and Fig. 8/Fig. S11, respectively).

In competition ELISA experiments, the interaction of the described binders with their immobilized target could be specifically inhibited by preincubation with free non-biotinylated target (Fig. 7b and Fig. S10b).

			Affinity					Selectivity
			BCL-2	BCL-XL	BCL-W	MCL-1	ERK2	
Selection type	Binder name	Target selection	K_D in nM	K_D in nM	K_D in nM	K_D in nM	K_D in nM	
One-round	008_H10	BCL-2	0.058	no binding	no binding	no binding		specific
One-round	008_C6	BCL-2	0.030	1.014*	2.919*	no binding		34
One-round	008_F2	BCL-2	0.523	85.600	no binding	no binding		164
One-round	008_D3	BCL-2	0.787	2.464*	2.757*	no binding		3
Three-round	001_C1	BCL-2	0.482	13.013*	no binding	no binding		27
Three-round	001_C10	BCL-2	0.194	no binding	23.100	no binding		119
Three-round	011_F12	BCL-2	0.557	10.600	7.020	no binding		13
Three-round	012_F12	BCL-XL	1.440	1.040	2.490	no binding		1
Three-round	003_D9	BCL-W	7.854*	5.447*	0.063	no binding		86
Three-round	003_C9	BCL-W	6.696*	1.303*	1.118*	no binding		1
Three-round	013_H8	BCL-W	no binding	6.830	0.643	no binding		11
Three-round	013_D12	BCL-W	no binding	26.600	10.300	no binding		3
Three-round	014_G9	MCL-1	no binding	no binding	no binding	0.774		specific
Four-round	4.3.E_E7	ERK2	no binding			no binding	4.793*	specific

Selectivity color code
specific
>100
>75
>25
>10
<5

Fig. 8. K_D matrix summarizing the affinity and selectivity determined by SPR for interactions between all targets and all binders. The kinetic data of the interactions were first evaluated with a global fit using the Langmuir [105] model. Regarding the interactions between binders and their original target used in the selection ("cognate target") (diagonal interactions highlighted by pink frames), the binding of 12 out of all 14 selected binders can be well described by a 1:1 Langmuir binding model. Only the 4.3.E_E7/ERK2 interaction and the 003_C9/BCL-W interaction were not fitted well by a 1:1 Langmuir binding model, and instead, a two-state binding model was used [106] (for details of the evaluation of different models, see Supplementary Results). Interactions of binders with other, non-cognate family members [indicated by an asterisk (*)] also required this more complicated model. In total, 55 binder/target interactions were investigated (Fig. S11). For extracted kinetic data, see Table 2 and Table ST2.

The affinities estimated from these experiments were confirmed with SPR measurements using a global kinetic fit (Table 2, Figs. 7c and 8, Table ST2 and Figs. S10c and S11). It should be noted that, if a binder interacts with more than one family member, the interaction with the target the binder was selected against is always the strongest (see also Supplementary Results).

Among the representative LoopDARPins, 001_C10, originating from the BCL-2 selection, for example, is a LoopDARPin that specifically binds to BCL-2 with an excellent K_D of 194 pM. From the BCL-XL selection, 012_F12 strongly binds to BCL-XL (K_D = 1 nM) and to BCL-2 (K_D = 1.4 nM) and slightly more weakly to BCL-W (K_D = 2.5 nM). 003_D9, originating from a selection against BCL-W, specifically binds to BCL-W with high affinity (K_D = 63 pM) and less strongly to BCL-XL (K_D = 5.5 nM) and to BCL-2 (K_D = 7.9 nM). The binder 014_G9 is specific for MCL-1, the target it was selected against, with a K_D of 774 pM.

One-round ribosome-display selections against BCL-2 using the N_{mix}-I-IL-IF-C_{mix} LoopDARPin library

The abovementioned results of having obtained specific picomolar binders in three rounds of ribosome display gave us confidence that, with LoopDARPins, very stringent selections might be possible. We chose to test this assumption by carrying out only one round of ribosome display with our naïve LD_$N_{mix}3C_{mix}$ LoopDARPin library against the target BCL-2, and this round would directly be an off-rate selection with 250-fold excess of non-biotinylated BCL-2 as competitor (Fig. 2). To compare the performance of our LD_$N_{mix}3C_{mix}$ LoopDARPin library to the conventional DARPin library without loop and without randomized caps [4,7], we conducted parallel selections on BCL-2 with these two libraries using identical experimental conditions.

A significant amount of reverse-transcribed RNA could be recovered over background using the LD_$N_{mix}3C_{mix}$ LoopDARPin library (Fig. S12), indicating the successful selection of binders after one round, while no recovery of reverse-transcribed RNA over background was observed using the conventional DARPin library without loop and without randomized caps during this very stringent selection procedure. Since this RNA enrichment can only serve as an indication, it was important to actually analyze single clones on the protein level. For the conventional DARPin library without loop and without randomized caps [4,7], 94 clones were screened by ELISA using crude *E. coli* extracts. However, none of the screened conventional DARPin clones showed binding to BCL-2 after a stringent one-round off-rate selection.

To assess the quality of the recovered LoopDARPins from this one-round selection, we screened 94 clones by ELISA using crude *E. coli* extracts. In contrast to the conventional DARPin library without loop, nine LoopDARPins (9.6%) showed specific binding to BCL-2 (signal/background $\geq$ 10). None of the analyzed LoopDARPins showed significant binding to microtiter plates coated with streptavidin and BSA.

The sequences of the nine initial hits all were found to be unique, in frame and containing no stop codons (data not shown). All nine LoopDARPins were IMAC purified and directly screened for the slowest off-rates by SPR at a concentration of 50 nM. The five most promising LoopDARPins were characterized by analytical SEC. LoopDARPins 008_H10, 008_F2 and 008_D3 were largely monomeric. 008_C6 was monomeric but also possessed an oligomeric fraction, whereas 008_F5 was mostly oligomeric (data not shown). Therefore, 008_F5 was excluded from further analyses. The interaction of the remaining four LoopDARPins with BCL-2 and with the other BCL-2 family members was further examined by ELISA and the exact K_D values were determined at multiple concentrations using SPR experiments.

The sequences of the final hits are shown in Fig. S9. Results for the representative LoopDARPins 008_H10 and 008_F2 from this one-round selection are shown in Table 2 and Figs. 7 and 8 (results for all LoopDARPins are shown in Table ST2 and Figs. S10 and S11). K_D values determined by SPR for interactions between all targets and all four LoopDARPins are summarized in Fig. 8.

Due to the fact that sequence and structure homology among the used BCL-2 family members is very high, selected LoopDARPins again bound to more than one member of the family but, as before, did not bind to MCL-1. LoopDARPins that bind with high affinity exclusively to BCL-2 are 008_H10 and 008_F2. 008_C6, and 008_D3 also bind with high affinity to other family members. Specificities determined by ELISA were consistent with results obtained from SPR measurements (Fig. 7a/Fig. S10a and Fig. 8/Fig. S11, respectively).

Binding of all LoopDARPins to BCL-2 could be blocked by preincubation of BCL-2 with an excess of free pD-BIM, indicating that, even without directing LoopDARPins toward the groove through a prepanning step, they bind near or into the groove (Fig. 7a and Fig. S10a). Both the surface-exposed groove and the randomized positions of all selected LoopDARPins, especially in the loop region, are enriched with hydrophobic residues (Fig. S9), suggesting an interaction of the loop with the groove. However, further analyses are necessary to test this hypothesis. The interaction of all tested LoopDARPins with BCL-2 could be specifically inhibited by preincubation with free non-biotinylated target, as determined by competition ELISA experiments (Fig. 7b and Fig. S10b), and estimated affinities were consistent with results obtained from SPR measurements (Table 2, Figs. 7c and 8, Table ST2 and Figs. S10c and S11).

LoopDARPins 008_H10 and 008_F2 exclusively bind BCL-2 with high affinity (K_D = 58 pM and 523 pM, respectively) and only 008_F2 also binds moderately to BCL-XL with a K_D of 85.6 nM. Both 008_C6 and 008_D3 bind to BCL-2, BCL-XL and BCL-W with the interaction to BCL-2 being the strongest (Fig. 8). Again, if a selected LoopDARPin binds more than one family member, the interaction with the target the binder was initially selected against, BCL-2, is the strongest (see also Supplementary Results). Most importantly, the two LoopDARPins with the highest affinity toward BCL-2 obtained from this one-round selection were 008_H10 and 008_C6 with K_D values of 58 and 30 pM, respectively (Table 2, Table ST2 and Fig. 8). This affinity is quite extraordinary for a one-round selection experiment.

LoopDARPins originating from four-, three- or one-round selections thus possess K_D values in the low nanomolar to mid-picomolar range (Table 2, Table ST2 and Fig. 8). LoopDARPins therefore constitute a large fraction of the highest affinity DARPins so far reported, and some of these were obtained after only one round of selection. This emphasizes the great potential of our new LoopDARPin design.

Selected LoopDARPins possess favorable biophysical properties

We performed in-depth biophysical analyses of three selected LoopDARPins. Expression, purity after single-step IMAC and storage stability were identical with unselected LoopDARPins (data not shown). SEC coupled to MALS revealed that all three selected LoopDARPins possess a clear monomeric species at a concentration of 1 mg/ml (50 μM) (Fig. 9a). However, the percentage of oligomeric species present varies, as observed for unselected LoopDARPins. LoopDARPin 001_C10 (randomized caps) is largely monomeric with a small dimer shoulder, and this shows that tightly binding, predominantly monomeric LoopDARPins can be obtained in selections. Nonetheless, 008_H10 (unrandomized caps) possesses additional peaks at lower retention volumes, identified as oligomeric species, and for 008_C6 (unrandomized caps), these oligomeric species are more pronounced. The CD spectra of the selected LoopDARPins superimpose well with the spectra of unselected LoopDARPins and conventional DARPins, confirming that their secondary structure contents are equal (Fig. S13). As for unselected LoopDARPins, the contribution of the additional amino acids from the loop is too small to affect the overall spectrum. GdmCl equilibrium unfolding experiments show midpoints of unfolding between 2.91 and 3.39 M GdmCl (Fig. 9b and Table 1), which compares well to values determined for unselected LoopDARPins and conventional DARPins (N3C LoopDARPins between 2.25 and 4.5 M GdmCl; N3C DARPins between 2.88 and 4.95 M GdmCl [12]). With respect to thermal unfolding, selected LoopDARPins tested show a single cooperative transition (Fig. 9b and Table 1). All selected LoopDARPins tested belong to the group (see above), which only show a first transition upon heating to 50–60 °C, where about 20–40% of the initial helical CD

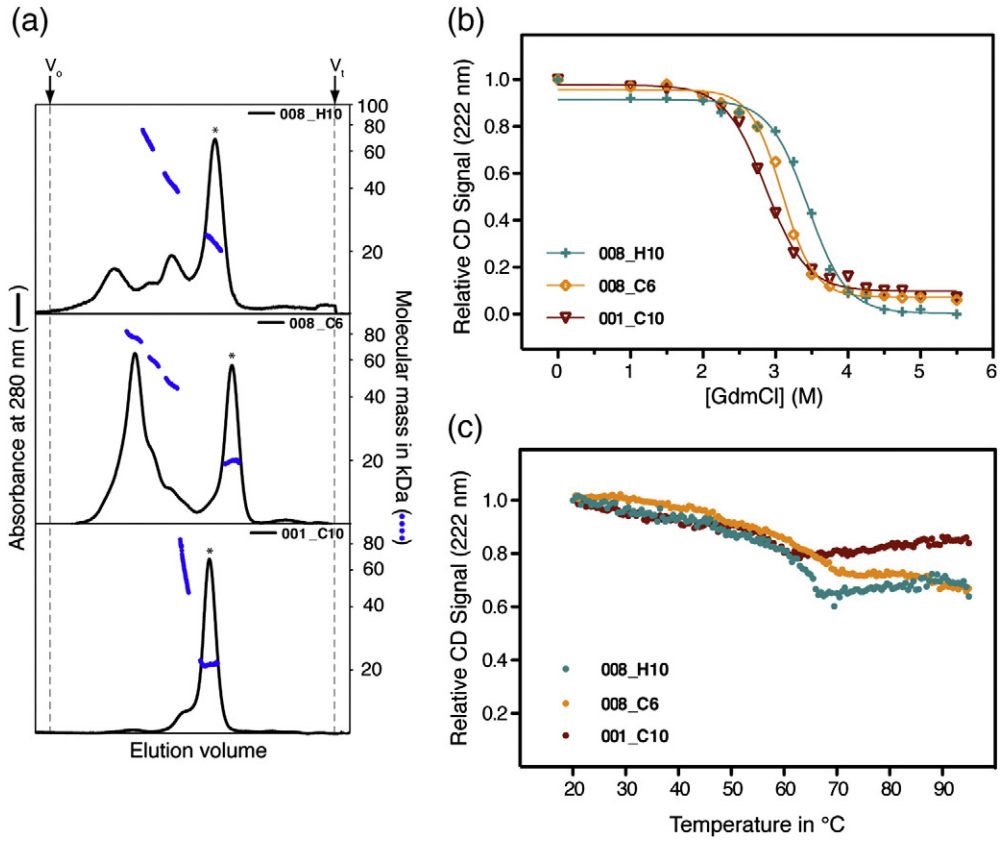

Fig. 9. (a) Monomeric or oligomeric state of three selected LoopDARPins, analyzed by SEC, coupled to MALS. For sequences of the LoopDARPins, see Fig. S9. The elution profiles represent the absorption at 280 nm (left-hand *y*-axis). Indicated by a line of blue dots across the eluting peaks, the right-hand *y*-axis shows the molecular weight of the eluting particles as determined by MALS. As an approximation, calculated molecular masses are as follows: monomer, 20 kDa; dimer, 40 kDa; trimer, 60 kDa; tetramer, 80 kDa. For exact calculated molecular weights of the monomer, see Table 1. Peaks corresponding to the monomeric species are denoted with an asterisk (*). The void volume (V_o = 10 ml) and the total volume (V_t = 24 ml) are indicated by gray broken lines in the graph. Two (008_H10 and 001_C10) out of three proteins are mainly monomeric at a concentration of 1 mg/ml (50 μM), whereas 008_C6 possesses a significant oligomeric fraction. 008_C6 is the most hydrophobic of the three LoopDARPins. As for unselected LoopDARPins, the obtained results underline that dimerization and oligomerization tendencies increase with increased hydrophobicity of the randomized positions. (b) Equilibrium unfolding and (c) thermal denaturation of the three selected LoopDARPins investigated in (a). (b) The equilibrium denaturation was followed by observing the CD signal at 222 nm as a function of [GdmCl] (see Materials and Methods). The CD signal is displayed as fraction of the CD value of each sample at 0 M GdmCl. The unfolding of the selected LoopDARPins tested cannot be well described by a two-state equilibrium system, and thus, no ΔG values are reported and the apparent midpoints of denaturation are summarized in Table 1. (b) The thermal denaturation was monitored by observing the CD signal at 222 nm. The CD signal is displayed as fraction of the CD value of each sample at 20 °C. The heating gradient was 1 °C/min and melting was only partially reversible [i.e., only 50% of the signal was regained upon cooling (data not shown)].

signal is lost. However, these LoopDARPins cannot be denatured further.

We thus conclude that the high degree of stability of DARPins [7] is retained in unselected and in selected LoopDARPins, underlining the success of our design.

Evaluation of the cap randomization strategy

To determine if certain cap variants were strongly enriched at the expense of others during selections, we compared their occurrence in the selected LoopDARPins to the cap distribution present in the naïve LD_$N_{mix}3C_{mix}$ LoopDARPin library. A detailed analysis can be found in Supplementary Results. Importantly, all cap variants and combinations (except for the N_{ran}–C_{old} combination, which is present in low frequency in the naïve library anyway) are present in the final hits. This indicates that having all cap combinations available is clearly beneficial and emphasizes the importance of our design strategy to provide addition diversity in the capping repeats.

Discussion

LoopDARPin design and characterization

Many studies demonstrated the ability of the original DARPin design to generate highly specific binders against numerous targets [4–6]. Nevertheless, we aimed at modifying DARPins toward different modes of target binding. By adding a long protruding loop to the scaffold, we sought to increase the conformational flexibility and the interaction surface of original DARPins. This reengineering should yield a scaffold with extended epitope binding properties.

To realize this notion, there were several obstacles to be overcome. First, the insertion of a long loop will naturally destabilize a given framework [108–110], since restricting the degrees of freedom of the loop upon folding constitutes a significant loss of entropy. By using loops with a defined stem, as in the antibody CDR-H3 loop and in natural ankyrin repeat proteins that possess loop insertions [23,35,43–46], we create additional interactions within this stem and between stem and DARPin framework, which greatly diminish this entropy loss upon folding. Inspired by nature, we employed sequence and structural analyses to identify a loop consensus sequence, composed of fixed stabilizing framework positions and randomized potential interaction positions. This loop could be placed into the existing DARPin scaffold without extensive reengineering of the DARPin framework. We found that, with this strategy, the stability of the created LoopDARPins is very similar to that of conventional DARPins.

Second, the insertion of a loop may create a clash with neighboring repeats, as it disrupts the otherwise orderly arrangement of the neighboring hairpin repeats that are connected through H-bonds. However, by designing a mutation in the repeat following the loop-containing one, this could be accommodated. More importantly, different conformations of the loop could be shown to be compatible with the repeat protein structure, such that the loop can sample different conformations.

Third, we had to define a randomization strategy for the loop. A balance had to be found to create a potential target interaction surface yet avoiding issues with folding of the protein. We chose a library containing all amino acids except cysteine but biased the library for Tyr, Ser and Gly, as this combination was known from the analysis of natural antibodies [58–60,62], natural protein–protein interactions [61] and previous library designs [48–56] to be compatible with this design goal. In the first installment of the library as described here, only a single loop length was used, but the same strategy can be extended in the future to a variable loop length, as in antibody CDR-H3 loops.

The interaction surface of LoopDARPins was further increased through a cap randomization strategy. The primary purpose of capping repeats [7,63] is to seal the hydrophobic interface that mediates the interactions between repeats at both ends of the molecule. We created both N- and C-caps with randomized residues. The inclusion of these randomized residues increases the total randomized surface further and thereby should specifically allow binding to those epitopes where binding is not possible with constant caps because of repulsive interactions. When tested for unfolding induced by heat or denaturants, a negative effect of cap randomization on overall stability was not observed, indicating that the chosen positions are not critical for stability and that the allowed residue types are compatible with the structure.

Finally, we also improved the library design at the nucleotide level, by placing defined restriction sites between repeats, which greatly facilitates the replacement of single repeats or caps, for example, for a localized mutagenesis strategy.

The analysis of unselected library members showed that our design largely preserved the favorable biophysical properties of DARPins. LoopDARPins can be expressed in large amounts in soluble form in *E. coli* and remain soluble and folded over weeks at 4 °C. Stability of LoopDARPins compare well to the stability of DARPins.

We did observe a tendency for dimerization and oligomerization of the LoopDARPins, however, which is much more rare in conventional DARPins. Several lines of evidence point to the fact that this is caused by the interactions of native molecules, through self-complementarity: (i) this is reversible by dilution, and monomer and oligomer peaks, isolated from a SEC run, regenerate all peaks, when re-injected (Figs. S4 and S5); (ii) the crystal structure directly shows these self-complementary loop and cap interactions in the crystal packing (Fig. 5b); (iii) the CD measurements do not hint at any decrease in helical content (Fig. S6 and Table 1); (iv) increased hydrophobicity in the cap region directly correlates with an increased dimerization and oligomerization tendency, but not with a decrease in stability (Fig. 4). Importantly, affinity and specificity are not compromised by this behavior. Moreover, it appears that the selected LoopDARPins show a higher percentage of monomers than the unselected library members, suggesting that stringent selection may favor this property.

While the current design of the library is attractive for applications in basic research or diagnostics, where the high affinity and rapid enrichment of specific binders can be exploited, we are aware that further refinements of the library design are necessary, before the LoopDARPins can be used for therapy: the same structural features that allow the selection of high-affinity binders in only one round of ribosome display, such as exposed and structurally adaptable loop residues, may also contribute to the increased self-complementarity leading to some

dimerization and oligomerization tendency of LoopDARPins. Future design cycles will have to fine-tune the balance between these two tendencies in order to retain the unparalleled fast enrichment of very specific, high-affinity binders yet diminish self-complementarity. Fortunately, the DARPin scaffold is very adaptable because of its intrinsic stability.

Rapid enrichment of binders with high affinity and specificity

An initial proof-of-principle selection against the kinase ERK2 with our first LoopDARPin library possessing fixed caps readily yielded a binder with low nanomolar K_D within four rounds of ribosome display (Table 2 and Figs. 7 and 8).

Subsequent selections were performed with our second LoopDARPin library possessing additional diversity in the capping repeats. This time, a family of proteins, the anti-apoptotic BCL-2 family, served as targets (Fig. 6 and Fig. S7). We were able to generate a toolbox of well-characterized binders against the family (Table 2, Figs. 7 and 8, Table ST2 and Fig. S9). Numerous LoopDARPins with affinities in the low nanomolar to mid-picomolar range were enriched within three rounds of ribosome display.

Selected LoopDARPins do not cross-interact with unrelated targets as shown by ELISA (Fig. 7a and Fig. S10a). We also verified that LoopDARPins per se do not bind to the investigated targets (Fig. 7b), as, for example, unselected LoopDARPins did not interact with ERK2 or any BCL-2 family member.

In a further selection against BCL-2, we increased selection stringency to its limit and directly performed a *single* ribosome-display off-rate selection round with our naïve LoopDARPin library with diversified caps. Unexpectedly, recovered LoopDARPins possessed affinities in the mid- to low picomolar range, with an affinity of even 30 pM for LoopDARPin 008_C6 (Table 2, Table ST2 and Fig. 8) obtained after only one round of ribosome display. With the use of identical highly stringent selection conditions, no binders were recovered after one round from the conventional DARPin library without loop and without randomized caps [4,7].

The affinities determined by SPR of all selected binders are in the low nanomolar to low picomolar range. The association rates are in the typical range for protein–protein interactions (10^4 to 10^6 M^{-1} s^{-1}) [111] and the dissociation rates range from 10^{-4} to 10^{-6} s^{-1} (10^{-2} s^{-1} when including also the measurements on non-cognate targets) (Table 2 and Table ST2). Selected binders possess biophysical properties (Table 1 and Fig. 9), which are in the same favorable range as for unselected LoopDARPins and conventional DARPins without loop [7,12].

We are aware of the fact that the observed recovery of high-affinity binders after only one round from our LoopDARPin library might be target- dependent. So far, we only compared the performance after one round of selection for our LoopDARPin library and the conventional DARPin library using BCL-2 as a target. Future comparative selections using additional targets have to show whether the improved recovery of binders during highly stringent selection conditions from our LoopDARPin library can be extended to other targets or at least to define the properties of favorable targets. Single-round selections resulting in such high-affinity and high-specificity binders would open the door to massively parallel selection strategies in a *common* liquid vessel, since the cumbersome elution and generation of the next-round library pool—which must be carried out for each target separately to maintain enrichment and thus requires *parallel* liquid handling—would become unnecessary, but they may also contribute to the high fraction of picomolar binders observed.

Cap randomization and selection

High-affinity LoopDARPins with unrandomized and randomized caps have been selected, showing that the introduction of our designed loop by itself is sufficient to generate highly specific binders with high affinity. Variants with unrandomized and randomized caps were selected from our second LoopDARPin library (containing diversified caps), illustrating that additional diversity with respect to capping repeats is clearly beneficial (Fig. S14). Interestingly, fewer binders with a randomized C-cap (C_{ran}) than expected have been selected. One reason for this observation might be the reduced availability of these binders during selections, perhaps because of the increased self-complementary upon cap randomization. This suggests that the selection might actually in itself enrich monomeric proteins. Fine-tuning of the randomization strategy will have to be addressed in future versions of the library, since increased hydrophobicity of capping repeats directly correlates with increased self-complementarity.

Targeting the BCL-2 family

We were able to generate BCL-2 and MCL-1-specific LoopDARPins as determined by ELISA and SPR (Fig. 7, Table ST2 and Figs. S10 and S11). In addition to that, we generated LoopDARPins, which specifically detect BCL-XL and BCL-W in ELISA setups (Fig. 7 and Fig. S10). However, future ribosome-display selections with an increased selection pressure toward specificity, for example, by rigorous prepanning with the undesired targets, may be used to generate LoopDARPins with improved specificity for BCL-XL and BCL-W.

The availability of our BCL-2 family binder toolbox (Fig. 8) may open up new possibilities in both basic and pharmaceutical research for either the detection or the inhibition of anti-apoptotic BCL-2 family members, since intracellular application of DARPins has recently been successfully shown [21,68].

With ELISA experiments, we can show that all selected binders bind to or near the target groove, as this interaction can be blocked by the preincubation with an excess of the natural groove ligand, the BH3-only peptide BIM (Fig. 7a and Fig. S10a). This is, at least to some degree, a consequence of the prepanning strategy (Fig. 2), which successfully directed the selected binders to this surface-exposed hydrophobic groove on the target (Fig. 6). However, LoopDARPins might possess an intrinsic property to bind to hydrophobic groove regions, possibly because of their conformationally flexible hydrophobic loop. Indeed, selected LoopDARPins from the one-round selection (which did not include a prepanning step) bound to or near the target groove (Fig. 7a and Fig. S10a).

Further experiments will have to test whether our LoopDARPins can also block this crucial interaction between anti-apoptotic and pro-apoptotic BCL-2 family members *in vivo*. If so, the selected binders could be used for intracellular applications to investigate the contribution of the BCL-2 family members in programmed cell death in more detail and could serve as a starting point for the development of future drugs.

We have not selected a binder, which binds to all anti-apoptotic BCL-2 family members with high affinity simultaneously. However, with LoopDARPin 008_C6, 012_F12 or 003_D9, for example, we have binders, which bind to three (BCL-2, BCL-XL and BCL-W) of the four family members at once. With 014_G9, we also have a LoopDARPin available, which binds with high affinity to MCL-1 (Fig. 8). With these two LoopDARPins, therefore, the family is essentially covered. With the many engineering options [6] of DARPins, we can not only work with mixtures but also fuse them to create bispecific molecules in different geometries—in the simplest case, through a flexible glycine–serine linker.

Conclusions

As we have shown here, LoopDARPins, which possess by design an increased interaction surface and a conformationally flexible paratope, enable us to select well-behaved and specific high-affinity binders against numerous targets with unparalleled speed. Enrichment of binders using LoopDARPins appears to be faster than with antibody single-chain Fv libraries [112] or with any other scaffold reported so far, even though there may be some influence of the target.

We believe that LoopDARPins extend the options of generating binders from this versatile scaffold for many applications, as they replace the strictly concave binding surface by one with a protrusion in the middle and even larger diversity, without compromising on protein stability. However, unlike in conventional DARPins, some increased self-complementary that will be addressed by a refinement of the current design still exists. Having LoopDARPins at hand, it is now possible to select specific high-affinity binders against targets using high stringency in combination with a minimal number of selection rounds, which makes LoopDARPins a valuable tool for high-throughput biotechnological binder generation.

Materials and Methods

In silico analyses

The GenBank[†] [113] and the PDB[‡] [114] databases were used in our analyses. Alignments were performed using ClustalX[§] [115] and BLAST[‖] [116]. InsightII (Accelrys, USA) was used for structural modeling.

Molecular dynamics simulations

All simulations were performed using the GROMOS simulation package [117,118]. Initially, the consensus LoopDARPin was relaxed in vacuum by energy minimization using a steepest descent algorithm. A reaction-field approach was used to treat the electrostatics. The cutoff for short-range and long-range pairlist constructions was 0.8 and 1.4 nm, respectively. The pairlist was updated every five steps. A step size of 2 fs was used. All bonds were constrained using the SHAKE algorithm [119] with a tolerance of 0.0001. The LoopDARPin was subsequently placed in a pre-equilibrated cubic box filled with simple point charge water molecules [120] (box size of 10.0 nm × 10.0 nm × 10.0 nm with 14,354 water molecules for a total of 44,711 atoms). The total charge of the protein is – 10 e; therefore, 10 sodium counterions were added to render the system electrostatically neutral. To mimic the experimental conditions (pH 7.4), we protonated Lys and Arg and the N-terminal amino group, while Glu and Asp and the C-terminal carboxyl group were deprotonated. The following equilibration step included raising the simulation temperature from 60 to 300 K while simultaneously decreasing the position restraint coupling constant from 25,000 kJ/mol/nm^2 to 0 kJ/mol/nm^2 in five equidistant steps for both temperature and coupling constant. At each equilibration step, a short 20-ps simulation at constant volume was carried out. Constant temperature was maintained by a Berendsen thermostat (coupling time of 0.1 ps) [121,122]. Initial velocities at a given temperature were taken from a Maxwell–Boltzmann distribution. Simulations were carried out for 50 ns using the GROMOS 45A4 force field [123], with periodic boundary conditions at a constant temperature of 300 K and constant pressure maintained by a Berendsen thermostat (coupling time of 0.1 ps) and barostat [coupling time of 0.5 ps and isothermal compressibility of 4.575×10^{-4} $(\text{kJ/mol/nm}^3)^{-1}$], respectively [121,122]. Structures were saved for analysis every 0.5 ps. RMSFs around the average structure were calculated after translational superposition of centers of mass and least-squares rotational fitting of atomic positions with respect to the equilibrated structure.

Molecular biology

Unless stated otherwise, all experiments were performed according to protocols found in Ref. [124]. Buffers and enzymes were from Fermentas (Germany) or New

England Biolabs (USA). The sequence of all oligonucleotides used can be found in Tables ST3–ST5.

Creation of ribosome-display format LoopDARPin libraries using novel ribosome-display vectors pRDV1 and pRDV3

pRDV1 contains unrandomized capping repeats N and C, whereas pRDV3 contains the N_{mix} and C_{mix} capping library mixtures (Supplementary Materials and Methods and Fig. S2). By ligation of the I-IL-IF core library (Supplementary Materials and Methods) into either pRDV1 or pRDV3 and by a PCR using this ligation mix as a template, capping repeats and flanking DNA regions necessary for ribosome display [42,64] were added to the core library. The N-I-IL-IF-C ribosome-display format library was created by cloning I-IL-IF via BstAPI/ApoI into pRDV1, followed by the PCR amplification of the ligation mix with oligonucleotides T7B and TolAk. The N_{mix}-I-IL-IF-C_{mix} ribosome-display format library was created accordingly via BstAPI/Bpu10I into pRDV3 (Fig. S2).

Antigen production vectors

Coding sequences for all BCL-2 family members and BIM were generated from oligonucleotides (Table ST4) using assembly PCR with Vent® Polymerase (1 min annealing at 50 °C and standard buffers). The coding sequence for ERK2 was PCR amplified from the vector NpT7-5His6_ERK2 [125] as template, using oligonucleotides pAT223_ERK2_f and pAT223_ERK2_r. For the expression of His-tagged, biotinylated ERK2 and BCL-2 family members, the resulting PCR products were cloned via BamHI/HindIII into pAT223-pD and pAT222-pD, respectively, to yield the expression vectors pAT223-pD_ERK2 and pAT222-pD_BCL-2, pAT222-pD_BCL-XL, pAT222-pD_BCL-W and pAT222-pD_MCL-1. His-tagged, biotinylated BIM peptide (BIM peptide sequence: MRPEIWIAQELRRIGDEFNAYYAR) used for prepanning was cloned via BamHI/HindIII into pAT223 [13,126] to yield the expression vector pAT223_BIM. For the expression of His-tagged, non-biotinylated BCL-2 family members (BCL-2, BCL-XL, BCL-W and MCL-1), the corresponding final PCR products were cloned via BamHI/HindIII into pPANK [7] to yield the expression vectors pPANK_BCL-2, pPANK_BCL-XL, pPANK_BCL-W and pPANK_MCL-1. NpT7-5His6_ERK2 was used for the expression of His-tagged, non-biotinylated ERK2. pAT223-pD constructs possess an Avi tag for biotinylation at the N-terminus, followed by a His_6 tag. pAT222-pD constructs carry an Avi tag for biotinylation at the N-terminus and a His_6 tag at the C-terminus. pPANK constructs possess an N-terminal MRGSHis_6 tag. pAT223 constructs possess an Avi tag for biotinylation at the N-terminus followed by protein D (pD) and a His_6 tag. pBirAcm (Avidity) was used for *in vivo* biotinylation.

LoopDARPin and antigen production and purification

For LoopDARPin protein expression, LoopDARPins were converted from the ribosome-display format through PCR amplification (oligonucleotides JSCRDif4 and WTC3n, for sequences, see Table ST3) and cloned into pPANK [7] via BamHI/HindIII. Stationary overnight XL1-Blue (Stratagene, USA) cultures (2YT, 1% glucose, 50 mg/l of ampicillin; 37 °C) were used to inoculate 1-l cultures (2YT, 50 mg/l of ampicillin; 37 °C) to an initial OD_{600} = 0.075. At OD_{600} = 0.8, the cultures were induced with 500 µM IPTG and incubated for 4 h. Cultures were centrifuged and the resulting pellets were resuspended in 35 ml of 50 mM Tris–HCl (pH 7.5), 500 mM NaCl, 10% glycerol and 20 mM imidazole and were sonicated. The lysates were re-centrifuged and proteins were purified over a Ni-nitrilotriacetic acid column (2 ml column volume) according to the manufacturer's instructions (Qiagen, Germany).

Expression of all ERK2 and BIM constructs was performed in *E. coli* BL21(DE3) (Stratagene, USA) at 30 °C. All other target constructs were expressed at 37 °C in *E. coli* XL1-Blue (Stratagene, USA). IMAC purification was performed as described for LoopDARPins. All buffers for target purification contained 2 mM 2-mercaptoethanol and purification was carried out at 4 °C. The biotinylated proteins ERK2, pD-BIM, BCL-2, BCL-XL, BCL-W and MCL-1 (plasmids pAT223-pD_ERK2, pAT223_BIM and pAT222-pD_BCL-2, pAT222-pD_BCL-XL, pAT222-pD_BCL-W, pAT222-pD_MCL-1) were produced using *in vivo* biotinylation with plasmid pBirAcm according to the protocols of Avidity and Qiagen. IMAC-purified, biotinylated protein was separated from non-biotinylated protein using anion-exchange chromatography. Prior to anion-exchange chromatography, proteins were dialyzed into low salt ion-exchange buffer [50 mM Hepes (pH 8.5), 200 mM NaCl, 10% glycerol and 1 mM DTT] and eluted with a linear gradient of high salt ion-exchange buffer [50 mM Hepes (pH 8.5), 400 mM NaCl, 10% glycerol and 1 mM DTT] at 4 °C, using an ÄKTAexplorer FPLC system with a Mono Q HR 5/50 column (GE Healthcare Biosciences, Pittsburg, USA). Non-biotinylated proteins were obtained as follows: IMAC-purified, non-biotinylated ERK2 (plasmid NpT7-5His6_ERK2) was purified using ion-exchange chromatography to remove phosphorylated ERK2. Non-biotinylated BCL-2, BCL-XL, BCL-W and MCL-1 (plasmids pPANK_BCL-2, pPANK_BCL-XL, pPANK_BCL-W and pPANK_MCL-1) were solely IMAC purified. To obtain non-biotinylated BIM for the use as competitor in competition ELISA experiments, we used the non-biotinylated anion-exchange fraction from the purification of the pAT223_BIM construct. The exact mass of all proteins was confirmed by mass spectrometry.

Size-exclusion chromatography

Analytical gel filtration was carried out at room temperature on an ÄKTAmicro FPLC system with a Superdex 75 PC 3.2/30 column (GE Healthcare Biosciences). Runs were performed with TBS_{150} [20 mM Tris–HCl (pH 7.5) and 150 mM NaCl] as running buffer at a flow rate of 60 µl/min. Moreover, correct folding of anti-apoptotic BCL-2 family members was analyzed through complex formation with a pD fusion of their natural BH3-only BIM peptide ligand using a Superdex 200 PC 3.2/30 column (GE Healthcare Biosciences).

SEC combined with MALS

The absolute mass of protein samples was determined using a liquid chromatography system (Agilent LC1100;

Agilent Technologies, Santa Clara, USA) coupled to an Optilab rEX refractometer (Wyatt Technology, Santa Barbara, USA) and a miniDAWN three-angle light-scattering detector (Wyatt Technology). For protein separation, a 24-ml Superdex 200 10/30 column (GE Healthcare Biosciences) was run in TBS_{150} (pH 7.5) at 0.5 ml/min. Analysis was performed using the ASTRA software (version 5.2.3.15; Wyatt Technology).

CD spectroscopy

CD spectra and heat denaturation curves were recorded on a Jasco J-715 instrument (Jasco, Japan) in TBS_{150} (pH 7.5) as described in Ref. [7] with a temperature shift from 20 °C to 95 °C within 75 min and a response time of 1 s. For equilibrium denaturation measurements in GdmCl, the unfolding of the LoopDARPins tested in the present study cannot be precisely described by a simple two- or three-state equilibrium system, and thus, no ΔG values are reported. To nevertheless estimate approximate denaturation midpoints, we analyzed equilibrium unfolding as previously described [12] and calculated them from the fit of the midpoints according to $D_{mx} = \Delta G_{0x}/m_x$, where x refers to the first or the second transition.

Crystallization and data collection

IMAC-purified $N_{ran}1\_G06\_C$ was separated by preparative SEC in TBS_{150} (pH 8.0) using an ÄKTAexplorer FPLC system with a Superdex 200 16/60 prep grade (GE Healthcare Biosciences). The monomeric fraction was subsequently concentrated to 5.3 mg/ml. Best-diffracting crystals were obtained by using the sitting-drop vapor diffusion method at 4 °C, in a 384-well crystallization plate. The drops contained 0.2 µl of protein and 0.2 µl of reservoir solution [0.1 M Na-cacodylate (pH 6.5), 0.2 M Li_2SO_4, 8% polyethylene glycol 20,000 and 8% polyethylene glycol 550 monomethyl ether], equilibrating with 30 µl reservoir. The crystals grew in 1–2 weeks from clear solution. Cryoprotection was achieved by adding glycerol to a final concentration of 10%. Diffraction data were collected at beamline PXI (X06SA) of the Swiss Light Source (Villigen, Switzerland) at a temperature of 90 K (see Table ST1 for data collection and refinement statistics). Data were recorded at 1 Å on a PILATUS 6M detector [127]. Images were processed with XDS [128]. The crystal belonged to space group $P2_12_12_1$. Assuming two molecules in the asymmetric unit, a Matthews coefficient of 2.27 $Å^3$/Da was calculated by using the molecular mass of 19,784 Da for a monomer, which corresponds to an estimated solvent content of 45.96%.

Molecular replacement, model building and refinement

The structure of $N_{ran}1\_G06\_C$ was solved by molecular replacement using PHASER molecular replacement [129] from within the CCP4 package [130] with a poly-Ala model missing the second internal β-turn of the consensus DARPin structure (PDB ID: 2XEE [47]) as a search model. Model building was carried out by using the program Coot [131]. The structure was refined using PHENIX [132]. The refinement protocol included anisotropic *B*-factors for all non-H atoms, occupancy refinement of atoms in alternative conformations and target weight optimization, resulting in a final model with an *R*-factor of 17.1% and an R_{free} of 19.7%. Stereochemical properties were analyzed with MolProbity [133] and WHATCHECK [134]. Structure figures were generated in PyMOL[¶].

Ribosome display

In vitro ribosome-display selections were performed as previously described [13,41,42]. All selections were performed in solution using 96-well deep plates on a King-Fisher Flex (Thermo Fisher Scientific, Rockford, USA). A ribosome-display round consisted of a 30-min prepanning step on streptavidin-coated magnetic beads (Dynabeads MyOne Streptavidin T1; Invitrogen, USA), a 1-h target binding step (panning) and a 30-min pull-down with streptavidin-coated magnetic beads. Stringency was increased through elongating washing steps after pull-down and/or through the addition of non-biotinylated target as competitor in off-rate selections after panning.

Target proteins were used at a final concentration of 250 nM. In off-rate selections, a final target concentration of 50 nM was used. Improved off-rates were achieved through the addition of a 250× molar excess of non-biotinylated target. Eluted mRNA was isolated using the SV Total RNA Isolation System (Promega) with a vacuum manifold. Eluted and purified mRNA was reverse transcribed into DNA using the oligonucleotide JSCRDir2 (5′-ATCTGCTTCGGCCTTCGCTTTAGCATCTGCCGC CGCTTTCG-3′) and amplified by PCR (oligonucleotides JSCRDif4 and JSCRDir2; see Table ST3).

Analysis of selected binders

DNA sequences were determined using standard techniques. Amino acid sequences of all final hits are listed in Fig. S9. For ELISA screening, cell pellets from 1-ml expression cultures were lysed with 50 µl B-PERII (Thermo Fisher Scientific) and lysates were mixed with 950 µl PBS-TB (pH 7.4) [PBS containing a final concentration of 0.1% (v/v) Tween 20 and 0.2% (w/v) BSA]. For quantitative ELISA, analytical gel-filtration, CD and SPR measurements, selected library members were produced on a liter scale and purified as described above.

ELISA

Biotinylated antigens were immobilized as follows: 384-well high binding microplates (Greiner Bio-One GmbH, Frickenhausen, Germany) were coated with 20 µl of streptavidin (66 nM in PBS) and blocked with 0.2% BSA (w/v) (44 µl PBS-TB). We immobilized 20 µl of 100 nM biotinylated target proteins (in PBS-TB supplemented with a final concentration of 1 mM DTT). For the screening of selected pools, 20 µl of 1:100 diluted crude extracts was applied to wells with or without immobilized antigen for 45 min at room temperature. After extensive washing, binding was detected with an anti-RGS-His antibody (Qiagen GmbH, Hilden, Germany; it specifically discriminates between the N-terminal RGS-His_6 tags of LoopDARPins and the C-terminal His_6 tag of the antigen), an anti-mouse

IgG-alkaline phosphatase conjugate (Pierce, Thermo Fisher Scientific) and *p*-nitrophenylphosphate (Sigma-Aldrich, Buchs, Switzerland). Quantitative ELISAs were performed in the same manner with purified LoopDARPins. For ELISAs where target specificity and groove binding was determined, binders were used at a final concentration of 5 nM.

Groove binding of LoopDARPins was assessed by a groove competition ELISA, where the immobilized target was incubated with a final concentration of 5 μM non-biotinylated pD-BIM possessing a His_6 tag (which does not cross-react with the anti-RGS-His antibody), like the antigen, for 1 h and during the LoopDARPin binding reaction. To exclude that the abolished binding of LoopDARPins to the target originates from interactions between LoopDARPin and pD-BIM, we also tested LoopDARPin binding to immobilized biotinylated pD-BIM (20 μl of 100 nM biotinylated pD-BIM).

For competition ELISAs, purified binders (final concentration, 2.5 nM) were incubated with increasing concentrations of non-biotinylated target for 1 h and during the binding reaction. All washing steps were performed with 40 μl PBS-T per well on an ELx405 microplate washer (BioTek, Winooski, USA). Dispensing steps were performed on a MicroFlo Select liquid dispenser (BioTek). Crude extracts were applied with a Liquidator96 system (Mettler-Toledo GmbH, Greifensee, Switzerland).

Surface plasmon resonance

Binding kinetics of selected binders were determined by SPR measurements on a ProteOn XPR36 instrument [135]. Experiments were performed in TBS_{150} with 0.005% Tween-20 at 15 °C (with biotinylated ERK2 as target) or at 20 °C (with biotinylated BCL-2 family members). Biotinylated target proteins (75 nM) were immobilized on a ProteOn NLC sensor chip. Interactions at intersecting spots were measured at an analyte flow of 100 μl/min with 10 min buffer flow stabilization, 4 min simultaneous analyte injection at five different concentrations using a logarithmic dilution series (0.5–50 nM) and a dissociation time of 2000 s with buffer flow. Signals obtained through the injection of buffer as analyte were subtracted from the measurements. Interspot reference data were used to correct data for bulk refractive index changes and baseline drifts. Binding curves were collected, processed and analyzed with the ProteOn Manager software (Bio-Rad Laboratories).

Protein Data Bank accession code

The atomic coordinates of LoopDARPin $N_{ran}1\_G06\_C$ were deposited in the PDB [114] (PDB ID: 4K5C).

Acknowledgments

We thank the members of the Plückthun laboratory for valuable discussions, Dr. H. Topal for his excellent help during unselected LoopDARPin characterization and the staff of beamline PXI at the Swiss Light Source for support during data collection. We thank Prof. Melanie H. Cobb (University of Texas Southwestern) for providing the NpT7-5His6_ERK2 vector template. J.S. was supported by a pre-doctoral fellowship of the Forschungskredit of the University of Zurich. This work was supported by the European Commission grant 268621 (NEXTBINDERS) and the Swiss National Science Foundation grant 3100A_146278/1 (both to A.P.).

Appendix A. Supplementary data

Supplementary data to this article can be found online at http://dx.doi.org/10.1016/j.jmb.2013.10.026.

Received 1 September 2013;
Received in revised form 17 October 2013;
Accepted 17 October 2013
Available online 24 October 2013

Keywords:
designed ankyrin repeat proteins;
protein design;
ribosome-display;
MAP kinase;
anti-apoptotic BCL-2 family

†http://www.ncbi.nlm.nih.gov/Genbank/
‡http://www.pdb.org
§http://www.clustal.org/
||http://www.ncbi.nlm.nih.gov/blast/
¶http://pymol.org/

Abbreviations used:
RMSF, root-mean-square fluctuation; IMAC, immobilized metal-ion affinity chromatography; SEC, size-exclusion chromatography; MALS, multi-angle light scattering; SPR, surface plasmon resonance.

References

[1] Uhlén M, Hober S. Generation and validation of affinity reagents on a proteome-wide level. J Mol Recognit 2009;22:57–64.
[2] Vaughan TJ, Williams AJ, Pritchard K, Osbourn JK, Pope AR, Earnshaw JC, et al. Human antibodies with subnanomolar affinities isolated from a large non-immunized phage display library. Nat Biotechnol 1996;14:309–14.
[3] Mondon P, Dubreuil O, Bouayadi K, Kharrat H. Human antibody libraries: a race to engineer and explore a larger diversity. Front Biosci 2008;13:1117–29.
[4] Binz HK, Amstutz P, Plückthun A. Engineering novel binding proteins from nonimmunoglobulin domains. Nat Biotechnol 2005;23:1257–68.
[5] Binz HK, Plückthun A. Engineered proteins as specific binding reagents. Curr Opin Biotechnol 2005;16:459–69.
[6] Boersma YL, Plückthun A. DARPins and other repeat protein scaffolds: advances in engineering and applications. Curr Opin Biotechnol 2011;22:849–57.

[7] Binz HK, Stumpp MT, Forrer P, Amstutz P, Plückthun A. Designing repeat proteins: well-expressed, soluble and stable proteins from combinatorial libraries of consensus ankyrin repeat proteins. J Mol Biol 2003;332:489–503.
[8] Bork P. Hundreds of ankyrin-like repeats in functionally diverse proteins: mobile modules that cross phyla horizontally? Proteins 1993;17:363–74.
[9] Li J, Mahajan A, Tsai M-D. Ankyrin repeat: a unique motif mediating protein–protein interactions. Biochemistry 2006;45:15168–78.
[10] Suzuki F, Goto M, Sawa C, Ito S, Watanabe H, Sawada J, et al. Functional interactions of transcription factor human GA-binding protein subunits. J Biol Chem 1998;273:29302–8.
[11] Malek S, Huxford T, Ghosh G. Ikappa Balpha functions through direct contacts with the nuclear localization signals and the DNA binding sequences of NF-kappaB. J Biol Chem 1998;273:25427–35.
[12] Kohl A, Binz HK, Forrer P, Stumpp MT, Plückthun A, Grütter MG. Designed to be stable: crystal structure of a consensus ankyrin repeat protein. Proc Natl Acad Sci USA 2003;100:1700–5.
[13] Binz HK, Amstutz P, Kohl A, Stumpp MT, Briand C, Forrer P, et al. High-affinity binders selected from designed ankyrin repeat protein libraries. Nat Biotechnol 2004;22:575–82.
[14] Amstutz P, Binz HK, Parizek P, Stumpp MT, Kohl A, Grütter MG, et al. Intracellular kinase inhibitors selected from combinatorial libraries of designed ankyrin repeat proteins. J Biol Chem 2005;280:24715–22.
[15] Amstutz P, Koch H, Binz HK, Deuber SA, Plückthun A. Rapid selection of specific MAP kinase-binders from designed ankyrin repeat protein libraries. Protein Eng Des Sel 2006;19:219–29.
[16] Zahnd C, Pecorari F, Straumann N, Wyler E, Plückthun A. Selection and characterization of Her2 binding-designed ankyrin repeat proteins. J Biol Chem 2006;281:35167–75.
[17] Zahnd C, Wyler E, Schwenk JM, Steiner D, Lawrence MC, McKern NM, et al. A designed ankyrin repeat protein evolved to picomolar affinity to Her2. J Mol Biol 2007;369:1015–28.
[18] Huber T, Steiner D, Röthlisberger D, Plückthun A. *In vitro* selection and characterization of DARPins and Fab fragments for the co-crystallization of membrane proteins: the Na(+)-citrate symporter CitS as an example. J Struct Biol 2007;159:206–21.
[19] Sennhauser G, Amstutz P, Briand C, Storchenegger O, Grütter MG. Drug export pathway of multidrug exporter AcrB revealed by DARPin inhibitors. PLoS Biol 2007;5:e7.
[20] Stefan N, Martin-Killias P, Wyss-Stoeckle S, Honegger A, Zangemeister-Wittke U, Plückthun A. DARPins recognizing the tumor-associated antigen EpCAM selected by phage and ribosome display and engineered for multivalency. J Mol Biol 2011;413:826–43.
[21] Kummer L, Parizek P, Rube P, Millgramm B, Prinz A, Mittl PRE, et al. Structural and functional analysis of phosphorylation-specific binders of the kinase ERK from designed ankyrin repeat protein libraries. Proc Natl Acad Sci USA 2012;109:E2248–57.
[22] Parizek P, Kummer L, Rube P, Prinz A, Herberg FW, Plückthun A. Designed ankyrin repeat proteins (DARPins) as novel isoform-specific intracellular inhibitors of c-Jun N-terminal kinases. ACS Chem Biol 2012;7:1356–66.
[23] Morea V, Tramontano A, Rustici M, Chothia C, Lesk AM. Conformations of the third hypervariable region in the VH domain of immunoglobulins. J Mol Biol 1998;275:269–94.
[24] Chothia C, Lesk AM. Canonical structures for the hypervariable regions of immunoglobulins. J Mol Biol 1987;196:901–17.
[25] Chothia C, Lesk AM, Tramontano A, Levitt M, Smith-Gill SJ, Air G, et al. Conformations of immunoglobulin hypervariable regions. Nature 1989;342:877–83.
[26] Tramontano A, Chothia C, Lesk AM. Framework residue 71 is a major determinant of the position and conformation of the second hypervariable region in the VH domains of immunoglobulins. J Mol Biol 1990;215:175–82.
[27] Brünger AT, Leahy DJ, Hynes TR, Fox RO. 2.9 Å resolution structure of an anti-dinitrophenyl-spin-label monoclonal antibody Fab fragment with bound hapten. J Mol Biol 1991;221:239–56.
[28] Wu S, Cygler M. Conformation of complementarity determining region L1 loop in murine IgG lambda light chain extends the repertoire of canonical forms. J Mol Biol 1993;229:597–601.
[29] Martin AC, Thornton JM. Structural families in loops of homologous proteins: automatic classification, modelling and application to antibodies. J Mol Biol 1996;263:800–15.
[30] Al-Lazikani B, Lesk AM, Chothia C. Standard conformations for the canonical structures of immunoglobulins. J Mol Biol 1997;273:927–48.
[31] Choi Y, Deane CM. Predicting antibody complementarity determining region structures without classification. Mol Biosyst 2011;7:3327–34.
[32] Kuroda D, Shirai H, Kobori M, Nakamura H. Structural classification of CDR-H3 revisited: a lesson in antibody modeling. Proteins 2008;73:608–20.
[33] Kabat EA, Wu TT, Perry HM, Gottesman KS, Foeller C. Sequences of proteins of immunological interest. NIH publication no 91-3242. Bethesda, MD: US Department of Health and Human Services. Public Health Service, National Institutes of Health; 1991.
[34] Rock EP. CDR3 length in antigen-specific immune receptors. J Exp Med 1994;179:323–8.
[35] Shirai H, Kidera A, Nakamura H. Structural classification of CDR-H3 in antibodies. FEBS Lett 1996;399:1–8.
[36] Segal DM, Padlan EA, Cohen GH, Rudikoff S, Potter M, Davies DR. The three-dimensional structure of a phosphorylcholine-binding mouse immunoglobulin Fab and the nature of the antigen binding site. Proc Natl Acad Sci USA 1974;71:4298–302.
[37] Sharon J. Structural correlates of high antibody affinity: three engineered amino acid substitutions can increase the affinity of an anti-*p*-azophenylarsonate antibody 200-fold. Proc Natl Acad Sci USA 1990;87:4814–7.
[38] Wilson IA, Stanfield RL. Antibody-antigen interactions: new structures and new conformational changes. Curr Opin Struct Biol 1994;4:857–67.
[39] Stanfield RL, Takimoto-Kamimura M, Rini JM, Profy AT, Wilson IA. Major antigen-induced domain rearrangements in an antibody. Structure 1993;1:83–93.
[40] Sela-Culang I, Alon S, Ofran Y. A systematic comparison of free and bound antibodies reveals binding-related conformational changes. J Immunol 2012;189:4890–9.
[41] Hanes J, Plückthun A. *In vitro* selection and evolution of functional proteins by using ribosome display. Proc Natl Acad Sci USA 1997;94:4937–42.
[42] Zahnd C, Amstutz P, Plückthun A. Ribosome display: selecting and evolving proteins *in vitro* that specifically bind to a target. Nat Methods 2007;4:269–79.
[43] Lishko PV, Procko E, Jin X, Phelps CB, Gaudet R. The ankyrin repeats of TRPV1 bind multiple ligands and modulate channel sensitivity. Neuron 2007;54:905–18.

[44] Jin X, Touhey J, Gaudet R. Structure of the N-terminal ankyrin repeat domain of the TRPV2 ion channel. J Biol Chem 2006;281:25006–10.
[45] McCleverty CJ, Koesema E, Patapoutian A, Lesley SA, Kreusch A. Crystal structure of the human TRPV2 channel ankyrin repeat domain. Protein Sci 2006;15:2201–6.
[46] Phelps CB, Huang RJ, Lishko PV, Wang RR, Gaudet R. Structural analyses of the ankyrin repeat domain of TRPV6 and related TRPV ion channels. Biochemistry 2008;47: 2476–84.
[47] Kramer MA, Wetzel SK, Plückthun A, Mittl PRE, Grütter MG. Structural determinants for improved stability of designed ankyrin repeat proteins with a redesigned C-capping module. J Mol Biol 2010;404:381–91.
[48] Fellouse FA, Wiesmann C, Sidhu SS. Synthetic antibodies from a four-amino-acid code: a dominant role for tyrosine in antigen recognition. Proc Natl Acad Sci USA 2004;101: 12467–72.
[49] Fellouse FA, Li B, Compaan DM, Peden AA, Hymowitz SG, Sidhu SS. Molecular recognition by a binary code. J Mol Biol 2005;348:1153–62.
[50] Fellouse FA, Barthelemy PA, Kelley RF, Sidhu SS. Tyrosine plays a dominant functional role in the paratope of a synthetic antibody derived from a four amino acid code. J Mol Biol 2006;357:100–14.
[51] Koide A, Gilbreth RN, Esaki K, Tereshko V, Koide S. High-affinity single-domain binding proteins with a binary-code interface. Proc Natl Acad Sci USA 2007;104:6632–7.
[52] Fellouse FA, Esaki K, Birtalan S, Raptis D, Cancasci VJ, Koide A, et al. High-throughput generation of synthetic antibodies from highly functional minimalist phage-displayed libraries. J Mol Biol 2007;373:924–40.
[53] Koide A, Tereshko V, Uysal S, Margalef K, Kossiakoff AA, Koide S. Exploring the capacity of minimalist protein interfaces: interface energetics and affinity maturation to picomolar K_D of a single-domain antibody with a flat paratope. J Mol Biol 2007;373:941–53.
[54] Birtalan S, Zhang Y, Fellouse FA, Shao L, Schaefer G, Sidhu SS. The intrinsic contributions of tyrosine, serine, glycine and arginine to the affinity and specificity of antibodies. J Mol Biol 2008;377:1518–28.
[55] Gilbreth RN, Esaki K, Koide A, Sidhu SS, Koide S. A dominant conformational role for amino acid diversity in minimalist protein–protein interfaces. J Mol Biol 2008;381: 407–18.
[56] Kossiakoff AA, Koide S. Understanding mechanisms governing protein–protein interactions from synthetic binding interfaces. Curr Opin Struct Biol 2008;18:499–506.
[57] Virnekäs B, Ge L, Plückthun A, Schneider KC, Wellnhofer G, Moroney SE. Trinucleotide phosphoramidites: ideal reagents for the synthesis of mixed oligonucleotides for random mutagenesis. Nucleic Acids Res 1994;22:5600–7.
[58] Kabat EA, Wu TT, Bilofsky H. Unusual distributions of amino acids in complementarity-determining (hypervariable) segments of heavy and light chains of immunoglobulins and their possible roles in specificity of antibody-combining sites. J Biol Chem 1977;252:6609–16.
[59] Padlan EA. On the nature of antibody combining sites: unusual structural features that may confer on these sites an enhanced capacity for binding ligands. Proteins 1990;7: 112–24.
[60] Mian IS, Bradwell AR, Olson AJ. Structure, function and properties of antibody binding sites. J Mol Biol 1991;217: 133–51.
[61] Lo Conte L, Chothia C, Janin J. The atomic structure of protein–protein recognition sites. J Mol Biol 1999;285: 2177–98.
[62] Collis AVJ, Brouwer AP, Martin ACR. Analysis of the antigen combining site: correlations between length and sequence composition of the hypervariable loops and the nature of the antigen. J Mol Biol 2003;325:337–54.
[63] Interlandi G, Wetzel SK, Settanni G, Plückthun A, Caflisch A. Characterization and further stabilization of designed ankyrin repeat proteins by combining molecular dynamics simulations and experiments. J Mol Biol 2008;375:837–54.
[64] Plückthun A. Ribosome display: a perspective. Methods Mol Biol 2012;805:3–28.
[65] Stumpp MT, Forrer P, Binz HK, Plückthun A. Designing repeat proteins: modular leucine-rich repeat protein libraries based on the mammalian ribonuclease inhibitor family. J Mol Biol 2003;332:471–87.
[66] Pace CN, Scholtz JM. Measuring the conformational stability of a protein. Protein structure: a practical approach; 1997 300–21.
[67] Barrick D, Baldwin RL. Three-state analysis of sperm whale apomyoglobin folding. Biochemistry 1993;32:3790–6.
[68] Kummer L, Hsu C-W, Dagliyan O, Macnevin C, Kaufholz M, Zimmermann B, et al. Knowledge-based design of a biosensor to quantify localized ERK activation in living cells. Chem Biol 2013;20:847–56.
[69] Lawrence MC, Jivan A, Shao C, Duan L, Goad D, Zaganjor E, et al. The roles of MAPKs in disease. Cell Res 2008;18: 436–42.
[70] Chen Z, Gibson TB, Robinson F, Silvestro L, Pearson G, Xu B, et al. MAP kinases. Chem Rev 2001;101:2449–76.
[71] Petros AM, Medek A, Nettesheim DG, Kim DH, Yoon HS, Swift K, et al. Solution structure of the antiapoptotic protein Bcl-2. Proc Natl Acad Sci USA 2001;98:3012–7.
[72] Feng W, Huang S, Wu H, Zhang M. Molecular basis of Bcl-xL's target recognition versatility revealed by the structure of Bcl-xL in complex with the BH3 domain of Beclin-1. J Mol Biol 2007;372:223–35.
[73] Denisov AY, Madiraju MSR, Chen G, Khadir A, Beauparlant P, Attardo G, et al. Solution structure of human BCL-w: modulation of ligand binding by the C-terminal helix. J Biol Chem 2003;278:21124–8.
[74] Fire E, Gullá SV, Grant RA, Keating AE. Mcl-1-Bim complexes accommodate surprising point mutations via minor structural changes. Protein Sci 2010;19:507–19.
[75] Denisov AY, Chen G, Sprules T, Moldoveanu T, Beauparlant P, Gehring K. Structural model of the BCL-w-BID peptide complex and its interactions with phospholipid micelles. Biochemistry 2006;45:2250–6.
[76] Green DR, Evan GI. A matter of life and death. Cancer Cell 2002;1:19–30.
[77] Troy CM, Salvesen GS. Caspases on the brain. J Neurosci Res 2002;69:145–50.
[78] Walker LSK, Abbas AK. The enemy within: keeping self-reactive T cells at bay in the periphery. Nat Rev Immunol 2002;2:11–9.
[79] Hengartner MO. The biochemistry of apoptosis. Nature 2000;407:770–6.
[80] Cory S, Adams JM. The Bcl2 family: regulators of the cellular life-or-death switch. Nat Rev Cancer 2002;2: 647–56.
[81] Rutledge SE, Chin JW, Schepartz A. A view to a kill: ligands for Bcl-2 family proteins. Curr Opin Chem Biol 2002;6: 479–85.

[82] Liang H, Fesik SW. Three-dimensional structures of proteins involved in programmed cell death. J Mol Biol 1997;274:291–302.
[83] Voutsadakis IA. Apoptosis and the pathogenesis of lymphoma. Acta Oncol 2000;39:151–6.
[84] Bairey O, Zimra Y, Shaklai M, Okon E, Rabizadeh E. Bcl-2, Bcl-X, Bax, and Bak expression in short- and long-lived patients with diffuse large B-cell lymphomas. Clin Cancer Res 1999;5:2860–6.
[85] Jäger R, Herzer U, Schenkel J, Weiher H. Overexpression of Bcl-2 inhibits alveolar cell apoptosis during involution and accelerates c-myc-induced tumorigenesis of the mammary gland in transgenic mice. Oncogene 1997;15:1787–95.
[86] Jäättelä M. Escaping cell death: survival proteins in cancer. Exp Cell Res 1999;248:30–43.
[87] Wilson JW, Nostro MC, Balzi M, Faraoni P, Cianchi F, Becciolini A, et al. Bcl-w expression in colorectal adenocarcinoma. Br J Cancer 2000;82:178–85.
[88] Shigemasa K, Katoh O, Shiroyama Y, Mihara S, Mukai K, Nagai N, et al. Increased MCL-1 expression is associated with poor prognosis in ovarian carcinomas. Jpn J Cancer Res 2002;93:542–50.
[89] Zhang B, Gojo I, Fenton RG. Myeloid cell factor-1 is a critical survival factor for multiple myeloma. Blood 2002;99:1885–93.
[90] Chonghaile TN, Letai A. Mimicking the BH3 domain to kill cancer cells. Oncogene 2008;27:S149–57.
[91] van Delft MF, Wei AH, Mason KD, Vandenberg CJ, Chen L, Czabotar PE, et al. The BH3 mimetic ABT-737 targets selective Bcl-2 proteins and efficiently induces apoptosis via Bak/Bax if Mcl-1 is neutralized. Cancer Cell 2006;10:389–99.
[92] Klasa RJ, Gillum AM, Klem RE, Frankel SR. Oblimersen Bcl-2 antisense: facilitating apoptosis in anticancer treatment. Antisense Nucleic Acid Drug Dev 2002;12:193–213.
[93] Kutzki O, Park HS, Ernst JT, Orner BP, Yin H, Hamilton AD. Development of a potent Bcl-x(L) antagonist based on alpha-helix mimicry. J Am Chem Soc 2002;124:11838–9.
[94] Tzung SP, Kim KM, Basañez G, Giedt CD, Simon J, Zimmerberg J, et al. Antimycin A mimics a cell-death-inducing Bcl-2 homology domain 3. Nat Cell Biol 2001;3:183–91.
[95] Becattini B, Kitada S, Leone M, Monosov E, Chandler S, Zhai D, et al. Rational design and real time, in-cell detection of the proapoptotic activity of a novel compound targeting Bcl-X(L). Chem Biol 2004;11:389–95.
[96] Kitada S, Leone M, Sareth S, Zhai D, Reed JC, Pellecchia M. Discovery, characterization, and structure-activity relationships studies of proapoptotic polyphenols targeting B-cell lymphocyte/leukemia-2 proteins. J Med Chem 2003;46:4259–64.
[97] Wang JL, Liu D, Zhang ZJ, Shan S, Han X, Srinivasula SM, et al. Structure-based discovery of an organic compound that binds Bcl-2 protein and induces apoptosis of tumor cells. Proc Natl Acad Sci USA 2000;97:7124–9.
[98] Degterev A, Lugovskoy A, Cardone M, Mulley B, Wagner G, Mitchison T, et al. Identification of small-molecule inhibitors of interaction between the BH3 domain and Bcl-xL. Nat Cell Biol 2001;3:173–82.
[99] Enyedy IJ, Ling Y, Nacro K, Tomita Y, Wu X, Cao Y, et al. Discovery of small-molecule inhibitors of Bcl-2 through structure-based computer screening. J Med Chem 2001;44:4313–24.
[100] Walensky LD, Kung AL, Escher I, Malia TJ, Barbuto S, Wright RD, et al. Activation of apoptosis *in vivo* by a hydrocarbon-stapled BH3 helix. Science 2004;305:1466–70.
[101] Baell JB, Huang DCS. Prospects for targeting the Bcl-2 family of proteins to develop novel cytotoxic drugs. Biochem Pharmacol 2002;64:851–63.
[102] O'Brien SM, Cunningham CC, Golenkov AK, Turkina AG, Novick SC, Rai KR. Phase I to II multicenter study of oblimersen sodium, a Bcl-2 antisense oligonucleotide, in patients with advanced chronic lymphocytic leukemia. J Clin Oncol 2005;23:7697–702.
[103] Shintani T, Klionsky DJ. Autophagy in health and disease: a double-edged sword. Science 2004;306:990–5.
[104] Lum JJ, DeBerardinis RJ, Thompson CB. Autophagy in metazoans: cell survival in the land of plenty. Nat Rev Mol Cell Biol 2005;6:439–48.
[105] Brookst I. Determination of rate and equilibrium binding constants for macromolecular interactions using surface plasmon resonance: use of nonlinear least squares analysis methods. Anal Biochem 1993;212:457–68.
[106] Futamura M, Dhanasekaran P, Handa T, Phillips MC, Lund-Katz S, Saito H. Two-step mechanism of binding of apolipoprotein E to heparin: implications for the kinetics of apolipoprotein E-heparan sulfate proteoglycan complex formation on cell surfaces. J Biol Chem 2005;280:5414–22.
[107] Chen L, Willis SN, Wei A, Smith BJ, Fletcher JI, Hinds MG, et al. Differential targeting of prosurvival Bcl-2 proteins by their BH3-only ligands allows complementary apoptotic function. Mol Cell 2005;17:393–403.
[108] Nagi AD, Regan L. An inverse correlation between loop length and stability in a four-helix-bundle protein. Folding Des 1997;2:67–75.
[109] Nagi AD, Anderson KS, Regan L. Using loop length variants to dissect the folding pathway of a four-helix-bundle protein. J Mol Biol 1999;286:257–65.
[110] Regan L. Protein redesign. Curr Opin Struct Biol 1999;9:494–9.
[111] Northrup S, Erickson H. Kinetics of protein-protein association explained by Brownian dynamics computer simulation. Proc Natl Acad Sci USA 1992;89:3338–42.
[112] Hanes J, Schaffitzel C, Knappik A, Plückthun A. Picomolar affinity antibodies from a fully synthetic naive library selected and evolved by ribosome display. Nat Biotechnol 2000;18:1287–92.
[113] Benson DA, Karsch-Mizrachi I, Lipman DJ, Ostell J, Rapp BA, Wheeler DL. GenBank. Nucleic Acids Res 2002;30:17–20.
[114] Berman HM, Battistuz T, Bhat TN, Bluhm WF, Bourne PE, Burkhardt K, et al. The Protein Data Bank. Acta Crystallogr Sect D Biol Crystallogr 2002;58:899–907.
[115] Larkin MA, Blackshields G, Brown NP, Chenna R, McGettigan PA, McWilliam H, et al. Clustal W and Clustal X version 2.0. Bioinformatics 2007;23:2947–8.
[116] Altschul SF, Gish W, Miller W, Myers EW, Lipman DJ. Basic local alignment search tool. J Mol Biol 1990;215:403–10.
[117] Schwab F, van Gunsteren WF, Zagrovic B. Computational study of the mechanism and the relative free energies of binding of anticholesteremic inhibitors to squalene-hopene cyclase. Biochemistry 2008;47:2945–51.
[118] van Gunsteren WF, Bakowies D, Baron R, Chandrasekhar I, Christen M, Daura X, et al. Biomolecular modeling: goals, problems, perspectives. Angew Chem Int Ed Engl 2006;45:4064–92.
[119] Ryckaert J-P, Ciccotti G, Berendsen HJC. Numerical integration of the cartesian equations of motion of a system with constraints: molecular dynamics of n-alkanes. J Comput Phys 1977;23:327–41.

[120] Berendsen HJC, Postma JPM, van Gunsteren WF, Hermans J. Interaction models for water in relation to protein hydration. In: Pullman B, editor. Intermolecular forces. Dordrecht: Reidel; 1981. p. 331–42.
[121] Berendsen HJC, Postma JPM, Van Gunsteren WF, DiNola A, Haak JR. Molecular dynamics with coupling to an external bath. J Chem Phys 1984;81:3684–90.
[122] van Gunsteren WF, Billeter SR, Eising AA, Hünenberger PH, Krüger P, Mark AE, et al. Biomolecular Simulation: the GROMOS96 manual and user guide; 1996.
[123] Schuler LD, Daura X, van Gunsteren WF. An improved GROMOS96 force field for aliphatic hydrocarbons in the condensed phase. J Comput Chem 2001;22:1205–18.
[124] Sambrook J, Fritsch EF, Maniatis T. Molecular cloning: a laboratory manual. 2nd ed. Cold Spring Harbor: Cold Spring Harbor Laboratory Press; 1989.
[125] Wilsbacher JL, Cobb MH. Bacterial expression of activated mitogen-activated protein kinases. Methods Enzymol 2001;332:387–400.
[126] Forrer P, Jaussi R. High-level expression of soluble heterologous proteins in the cytoplasm of *Escherichia coli* by fusion to the bacteriophage lambda head protein D. Gene 1998;224:45–52.
[127] Broennimann C, Eikenberry EF, Henrich B, Horisberger R, Huelsen G, Pohl E, et al. The PILATUS 1M detector. J Synchrotron Radiat 2006;13:120–30.
[128] Kabsch W. XDS. Acta Crystallogr Sect D Biol Crystallogr 2010;66:125–32.
[129] McCoy AJ, Grosse-Kunstleve RW, Adams PD, Winn MD, Storoni LC, Read RJ. Phaser crystallographic software. J Appl Crystallogr 2007;40:658–74.
[130] Collaborative Computational Project, Number 4. The CCP4 suite: programs for protein crystallography. Acta Crystallogr Sect D Biol Crystallogr 1994;50:760–3.
[131] Emsley P, Lohkamp B, Scott WG, Cowtan K. Features and development of Coot. Acta Crystallogr Sect D Biol Crystallogr 2010;66:486–501.
[132] Adams PD, Afonine PV, Bunkóczi G, Chen VB, Davis IW, Echols N, et al. PHENIX: a comprehensive Python-based system for macromolecular structure solution. Acta Crystallogr Sect D Biol Crystallogr 2010;66:213–21.
[133] Davis IW, Leaver-Fay A, Chen VB, Block JN, Kapral GJ, Wang X, et al. MolProbity: all-atom contacts and structure validation for proteins and nucleic acids. Nucleic Acids Res 2007;35:W375–83.
[134] Hooft RW, Vriend G, Sander C, Abola EE. Errors in protein structures. Nature 1996;381:272.
[135] Bravman T, Bronner V, Lavie K, Notcovich A, Papalia GA, Myszka DG. Exploring “one-shot” kinetics and small molecule analysis using the ProteOn XPR36 array biosensor. Anal Biochem 2006;358:281–8.